Progress in Oceanography 219 (2023) 103135

Contents lists available at ScienceDirect

Progress in Oceanography

journal homepage: www.elsevier.com/locate/pocean

Tagging of Atlantic bluefin tuna off Ireland reveals use of distinct oceanographic hotspots

Camille M.L.S. Pagniello [a,*], Niall Ó Maoiléidigh [b], Hugo Maxwell [b], Michael R. Castleton [a], Emilius A. Aalto [a], Jonathan J. Dale [a], Robert J. Schallert [a], Michael J.W. Stokesbury [c], Ronán Cosgrove [d], Simon Dedman [a], Alan Drumm [b], Ross O'Neill [b], Barbara A. Block [a]

[a] Oceans Department, Stanford University, Pacific Grove, CA 93950, United States
[b] Marine Institute, Newport Co. Mayo F28 PF65, Ireland
[c] Department of Biology, Acadia University, 33 University Avenue, Wolfville, Nova Scotia B4P 2R6, Canada
[d] An Bord Iascaigh Mhara, Irish Sea Fisheries Board, New Docks, Co. Galway, Ireland

ARTICLE INFO

Keywords:
Atlantic bluefin tuna
Pop-up satellite archival tagging
Oceanography
North Atlantic Current
Anticyclonic features
Newfoundland Basin

ABSTRACT

Electronic tagging of Atlantic bluefin tuna (ABT; *Thunnus thynnus*) has shaped our understanding of their movements and migrations throughout the Atlantic basin. In this study, we used pop-up satellite archival tagging data to examine the movements of 51 large (CFL $\mu \pm \sigma$: 215 ± 15 cm) ABT tagged off the coast of Ireland. When combined with satellite oceanographic data, we found that ABT take advantage of the warm North Atlantic Current to access foraging areas in the North Atlantic Ocean. We identified four potential foraging regions: (1) off the coast of Ireland, (2) the Bay of Biscay, (3) the Newfoundland Basin, and (4) the West European Basin. In addition, 14 ABT migrated to their spawning grounds in the Mediterranean Sea, entering by May 16 and exiting by July 7, on average. In all five regions, anticyclonic ocean features (i.e., eddies or recirculation) were present. In the open ocean, these features often co-occurred with areas where the daily maximum depth of tuna exceeded 400 m and tuna spent extended time at mesopelagic depths (i.e., greater than 200 m). We hypothesize that ABT exploit anticyclonic structures to forage on the abundant mesopelagic fish communities. Additionally, our results suggest that ABT are travelling across the North Atlantic Ocean in a directed migration to the Newfoundland Basin to reach what may be one of the best mesopelagic feeding grounds in the world.

1. Introduction

Atlantic bluefin tuna (ABT) (*Thunnus thynnus*) are one of the world's largest teleost predators, primarily inhabiting the waters of the North Atlantic Ocean (NAO) (Gibbs and Collette, 1967; Walli et al., 2009). They are highly sought after by fishers of many nations and are part of one of the highest-valued commercial fisheries in the world (McKinney et al., 2020). The International Commission for the Conservation of Atlantic Tunas (ICCAT) currently manages ABT as two populations, separated by the 45 °W meridian (Porch et al., 2019). Spawning grounds for these two ABT stocks are in the Gulf of Mexico and the Mediterranean Sea. More recently, a third spawning ground has been identified in the Slope Sea (Aalto et al., 2023; Richardson et al., 2016). Overfishing decimated ABT populations in the 1960s through the 2010s, but increased regulation of the fishing fleets and lower quotas have progressively enabled a recovery of the eastern ABT population.

At the start of the new millennium, ABT were reported in higher numbers off the west coast of Ireland, where they had previously only been reported sporadically. A recreational fishery was developed in September 2000, where 74 captures were made by rod and reel by the end of 2004 (Cosgrove et al., 2008). Tagging efforts off the coast of Ireland in 2003 and 2004 showed that ABT in Irish waters traveled to the Mediterranean spawning grounds as well as foraging areas in the western North Atlantic (Stokesbury et al., 2007). However, catches declined significantly and few ABT were recorded after 2005, making tagging operations challenging. ABT returned to Irish waters in 2014. This enabled an intensive, multi-national electronic tagging program off the west coast of Ireland between 2016 and 2020 whose goal was to provide a better understanding of the movements of large ABT tagged off the coast of Ireland occupying waters throughout the NAO as well as the Mediterranean Sea (Horton et al., 2020; Ó Maoiléidigh et al., 2016). ABT are now regularly captured by commercial and recreational fishers throughout their eastern Atlantic historic range, including in Denmark

* Corresponding author.
E-mail address: cpagniel@stanford.edu (C.M.L.S. Pagniello).

https://doi.org/10.1016/j.pocean.2023.103135
Received 1 December 2022; Received in revised form 5 September 2023; Accepted 2 October 2023
Available online 4 October 2023

Nomenclature

List of Acronyms

A	Eddy Amplitude (cm)
ABT	Atlantic bluefin tuna
ACE	Anticyclonic Eddies
ADT	Absolute Dynamic Topography
AMOC	Atlantic Meridional Overturning Circulation
ANOVA	Analysis of Variance
BoB	Bay of Biscay
CE	Cyclonic Eddies
CFL	Curved Fork Length
CI	Coastal Ireland
DSL	Deep Scattering Layer
EKE	Eddy Kinetic Energy
ICCAT	International Commission for the Conservation of Atlantic Tunas
KW	Kruskal-Wallis
L_s	Eddy Speed Radius (km)
MAD	Median Absolute Deviation
Med	Mediterranean Sea
MFZ	Maxwell Fracture Zone
MLD	Mixed Layer Depth
NAC	North Atlantic Current
NAO	North Atlantic Ocean
NB	Newfoundland Basin
NBRG	Newfoundland Basin Recirculation Gyre
PAT	Pop-up Archival Transmitting
PDT	PAT-style Depth-Temperature
PSAT	Pop-up Satellite Archival Transmitting
SSM	State Space Model
SST	Sea Surface Temperature
U_{avg}	Eddy Average Axial Speed (cm/s)
WEB	West European Basin
$\tilde{x}$	Median

(MacKenzie et al., 2020) and Norway (Ferter et al., 2019), indicating a strong recovery of the eastern stock is underway.

Electronic tags have enabled the tracking of marine top predators in relation to oceanographic features. Ocean currents often serve as highways for movements across ocean basins and thus define the spatial extent of some top predators. For example, the route of Pacific bluefin tuna during their *trans*-Pacific migration is related to seasonal shifts in latitude of the Subarctic Frontal Zone (Fujioka et al., 2018; Kitagawa et al., 2009). Additionally, many top predators utilize mesoscale eddies as feeding grounds. While cyclonic eddies (CEs) are often viewed as biological hotspots due to an increase in surface primary productivity within their boundaries (Falkowski et al., 1991), there is increasing evidence that clockwise-rotating anticyclonic eddies (ACEs) support rich mesopelagic (i.e., depths greater than 200 m) fish communities despite the transport of warm, nutrient-poor waters from the surface to deeper depths (Della Penna and Gaube, 2020; Devine et al., 2021; Fennell and Rose, 2015; Wang et al., 2023). Thus, it is hypothesized that ACEs may act as a conduit for both ectothermic and endothermic top predators to forage at deeper depths without surpassing their physiological limits including blue sharks (*Prionace glauca;* Braun et al., 2019), white sharks (*Carcharodon carcharias;* Gaube et al., 2018), northern elephant seals (*Mirounga angustirostris*; Keates et al., 2022) and loggerhead sea turtles (*Caretta caretta;* Gaube et al., 2017) as well as a variety of tunas and billfishes (Arostegui et al., 2022; Luo et al., 2015).

To increase our understanding of the use of oceanographic features by large ABT, we combined data collected by 51 electronically tagged ABT off the coast of Ireland between 2003 and 2020 with satellite oceanographic data characterizing the distribution and properties of mesoscale eddies. Tags collected light, temperature and depth data that were used to reconstruct the movement of ABT throughout the NAO via light-based geolocation. Our aims were to (1) map the migration patterns of large ABT, (2) examine how their horizontal spatial distribution was related to ocean currents and eddies, and (3) quantify the relationship between their vertical diving behavior and absolute dynamic topography (ADT), which we used as a proxy for some permanent, quasi-stationary, mesoscale anticyclonic eddies with clear climatological signatures.

2. Methods

2.1. Capture and satellite tagging

ABT were tagged in partnership with recreational anglers on the shelf of Donegal Bay or Courtmacsherry Bay in seven different years (2003, 2004, 2016 to 2020) (Table 1). ABT were captured using hook and line methods that included the use of trolling squid spreader bars. Once a fish was caught and reeled to the vessel, it was brought onboard using a titanium lip hook and a ramp specifically built for the vessel (Stokesbury et al., 2007; Wilson et al., 2015). Once onboard the boat, a saltwater hose was used to irrigate the fish's gills and a wet cloth was placed over the eyes. Curved fork length (CFL) and half girth measurements were taken as well as genetic samples from dorsal or anal fin clips. All work was conducted in accordance with Stanford University's Institutional Animal Care and Use Committee protocols. Since 2016, an animal welfare license has been required for tagging and was obtained from the Health Products Regulating Authority of Ireland (Project License AE19121/P003).

Three types of pop-up archival transmitting (PAT) or pop-up satellite archival transmitting (PSAT) tags (i.e., PAT4 mk10, miniPAT; Wildlife Computers, Inc., WA, USA and PSATFLEX; Lotek Wireless, Inc., ON, Canada) were used in this study. Attachment methods evolved over the deployment years, continuously improving long-term tag retention. All tags were placed about 15 cm into the dorsal musculature of the fish using a custom-built titanium tag dart and application tip (Wilson et al., 2015). Tag placement was primarily below the leading edge or center of the second dorsal fin. In 2003 and 2004, PAT4 mk10 tags were used. These tags recorded light, pressure (depth), and temperature data every 60 seconds. While PAT4 mk10 tags were often attached to the fish with a single titanium dart, without an extra tether loop, both miniPAT and PSATFLEX tags were attached to the fish at a second point with a custom-built loop to keep the tag closer to the fish. The miniPAT tags used since 2016 set their own archival sampling rate ranging from 3 to 5 seconds based on the number of days to pop-up. PSATFLEX tags archive data at a 10-second sampling rate, but are also able to transmit light, pressure, and temperature data at a 5-minute interval. In certain years, tags were set to release prior to reaching their crush depth, which varied from 1,200 m to 1,700 m based on their programming. However, this function was eventually turned off as some ABT dove deeper than the crush depth and tags accidentally released.

A total of 84 ABT were tagged off Ireland between 2003 and 2020, 61% of which were used in the analyses. During these deployments, some tags failed due to manufacturer issues. Some non-reporting and premature releases from Wildlife Computers, Inc. tags were due to a series of nosecone design changes starting in 2017 as well as battery failures in 2018. Lotek Wireless, Inc. were developed concurrently with deployments. Design problems with PSATFLEX tags, which at the time of deployment were entirely experimental, including battery passivation, post-release failures and excessive fouling which impeded the detachment of the tag and/or transmission of data.

Table 1
Metadata for 51 tags deployed off Ireland between 2003 and 2020 used in the analyses.

TOPP ID	Tagging Date	Deployment Latitude (°N)	Deployment Longitude (°W)	Curved Fork Length (cm)	Tag Model	Pop-Up Date	Pop-Up Latitude (°N)	Pop-Up Longitude (°W)	Track Start Date	Track End Date	Total Track Days	Straight Line Distance (km)
5103448	9/20/03	55.355	−7.519	221	PAT4 mk10	3/23/04	25.672	−67.390	9/20/03	3/23/04	186	5795
5103449	9/20/03	55.355	−7.519	225	PAT4 mk10	4/12/04	38.170	−13.540	9/20/03	4/12/04	206	1961
5104559	10/8/04	55.417	−7.467	230	PAT4 mk10	6/11/05	31.570	17.420	10/8/04	6/11/05	247	2766
5116030	10/9/16	54.532	−8.803	216	miniPAT	1/23/17	39.817	−41.476	10/9/16	1/23/17	107	2928
5116031	10/9/16	54.528	−8.792	216	miniPAT	6/26/17	42.376	−50.914	10/9/16	6/26/17	261	3334
5116032	10/11/16	54.544	−8.739	224	miniPAT	7/31/17	63.688	−4.166	10/11/16	7/31/17	294	1052
5116034	10/11/16	54.534	−8.822	220	miniPAT	8/5/17	35.851	14.644	10/11/16	6/5/17	238	2750
5116035	10/12/16	54.541	−8.781	206	miniPAT	6/25/17	34.014	12.740	10/12/16	6/25/17	257	2832
5116036	10/12/16	54.551	−8.816	215	miniPAT	7/1/17	47.045	−9.182	10/18/16	7/1/17	257	835
5116038	10/12/16	54.530	−8.810	199	miniPAT	10/13/17	54.501	−10.624	10/12/16	6/1/17	233	117
5116039	10/22/16	54.527	−8.632	206	miniPAT	3/6/17	44.090	−26.628	10/22/16	3/6/17	136	1741
5116040	10/25/16	54.714	−8.867	207	miniPAT	1/8/17	45.066	−41.522	10/25/16	1/8/17	76	2550
5116041	10/28/16	54.705	−8.859	224	miniPAT	9/2/17	61.105	−16.177	10/29/16	6/26/17	241	833
5116042	10/29/16	54.738	−8.822	240	miniPAT	5/19/17	27.558	−15.793	10/29/16	5/19/17	203	3071
5116043	10/29/16	54.761	−8.822	234	miniPAT	9/2/17	56.299	−7.938	10/29/16	9/2/17	309	180
5116044	10/29/16	54.782	−8.807	220	miniPAT	3/10/17	39.775	−42.040	10/29/16	3/10/17	133	2974
5117022	9/21/17	54.591	−8.677	229	miniPAT	2/22/18	45.212	−29.650	9/21/17	2/22/18	155	1821
5117023	10/27/17	54.902	−8.691	217	miniPAT	10/21/18	48.768	−19.736	10/27/17	6/20/18	237	2058
5117024	10/27/17	54.919	−8.697	228	miniPAT	4/2/18	35.460	−25.441	10/27/17	2/18/18	115	2517
5117025	10/30/17	54.802	−8.638	234	miniPAT	5/15/18	45.731	−30.478	10/30/17	5/15/18	198	1843
5117026	10/30/17	54.792	−8.642	235	miniPAT	3/10/18	51.578	−11.483	10/30/17	3/10/18	132	406
5117027	9/24/17	54.594	−8.750	176	miniPAT	1/15/18	40.345	−16.907	9/24/17	1/15/18	114	1696
5117028	9/25/17	55.048	−8.656	184	miniPAT	9/26/18	49.048	−7.892	9/25/17	5/16/18	234	670
5117029	9/25/17	55.044	−8.668	215	miniPAT	9/26/18	53.006	−10.843	9/25/17	5/18/18	236	269
5117030	9/26/17	54.562	−8.595	218	miniPAT	7/8/18	36.336	−6.572	9/26/17	1/26/18	123	2032
5118048	9/29/18	54.538	−8.822	212	miniPAT	9/23/19	53.246	−10.321	9/29/18	5/5/19	219	174
5118049	9/29/18	54.526	−8.816	188	miniPAT	11/3/18	49.289	−11.002	9/29/18	11/3/18	36	602
5118050	9/29/18	54.521	−8.826	228	miniPAT	11/9/18	43.790	−4.205	9/29/18	11/9/18	42	1239
5118051	9/29/18	54.521	−8.826	221	miniPAT	12/5/18	44.127	−8.390	9/29/18	12/5/18	68	1156
5118052	10/12/18	54.495	−8.905	220	miniPAT	10/14/19	35.889	14.658	2/20/19	9/21/19	214	2748
5118053	10/14/18	54.523	−8.769	217	miniPAT	6/27/19	40.129	3.420	10/14/18	6/27/19	257	1841
5118054	10/14/18	54.515	−8.821	189	miniPAT	5/16/19	41.064	−62.328	10/14/18	5/16/19	215	4161
5118056	10/14/18	54.523	−8.769	220	miniPAT	10/15/19	57.366	−8.180	10/14/18	6/1/19	231	319
5118057	10/14/18	54.561	−8.899	195	miniPAT	10/15/19	43.302	−69.837	10/14/18	10/15/19	367	4484
5118058	10/14/18	54.558	−8.903	223	miniPAT	10/15/19	59.194	−3.849	10/14/18	10/15/19	367	600
5118061	10/15/18	54.535	−8.888	217	miniPAT	10/16/19	59.132	−3.605	10/15/18	10/16/19	367	604
5119050	10/31/19	54.491	−8.720	215	miniPAT	8/3/20	50.717	−15.532	10/31/19	8/3/20	278	624
5120051	8/14/20	54.593	−8.896	205	PSATFLEX	12/12/20	45.576	−40.267	8/14/20	12/9/20	118	2458
5120053	8/27/20	54.639	−8.956	221	PSATFLEX	4/24/21	31.162	−21.333	8/27/20	4/21/21	231	2787
5120054	8/27/20	54.603	−8.940	210	PSATFLEX	4/24/21	47.149	−15.138	8/27/20	4/21/21	235	935
5120057	8/28/20	54.607	−8.837	231	PSATFLEX	8/28/21	40.859	0.852	8/28/20	5/29/21	275	1689
5120059	9/15/20	54.576	−8.829	170	miniPAT	9/16/21	55.395	−8.062	9/15/20	9/16/21	367	104
5120061	9/16/20	54.587	−8.899	210	miniPAT	7/14/21	46.422	−5.464	9/16/20	7/13/21	298	941
5120063	9/20/20	54.599	−8.665	232	PSATFLEX	5/23/21	30.948	−43.973	9/20/20	5/15/21	218	3834
5120064	9/20/20	54.577	−8.931	220	PSATFLEX	3/19/21	44.114	−37.370	9/20/20	3/15/21	177	2348
5120065	9/20/20	54.582	−8.909	212	PSATFLEX	7/17/21	44.851	−41.510	9/20/20	7/15/21	299	2558
5120067	9/20/20	54.561	−8.943	214	miniPAT	7/18/21	47.914	−39.780	9/20/20	7/18/21	302	2256
5120069	9/21/20	54.635	−8.936	202	PSATFLEX	7/18/21	46.043	−43.257	9/21/20	7/16/21	299	2591
5120071	9/29/20	51.565	−8.634	232	miniPAT	9/30/21	51.445	−8.527	9/29/20	9/30/21	367	15
5120072	9/29/20	51.575	−8.585	217	miniPAT	6/2/21	42.362	−24.926	9/29/20	6/2/21	247	1604
5120075	10/12/20	51.563	−8.623	200	miniPAT	11/29/20	43.552	−2.441	11/1/20	11/29/20	29	1004

2.2. Geolocation methods

We estimated daily locations of tagged ABT via light-based geolocation (Hill, 1994) and generated most probable tracks with 95% confidence intervals for each tag using a Bayesian state space model (SSM; Block et al., 2011; Jonsen et al., 2005; Teo et al., 2004; Wilson et al., 2015). The Bayesian SSM uses light-level longitudes, sea surface temperature-based latitudes and bathymetry to estimate daily positions of tagged animals while accounting for observation error and standardizing location estimates in time. Tracks and temperature-depth time series were reviewed and cropped to remove poor-quality or data-absent sections. This included tracks that ended before the pop-up date as the tags were either recovered or light, pressure and/or temperature data ended prior to the pop-up date in addition to tracks with large longitude gaps at the start and throughout the deployment.

2.3. Hotspot identification

The total number of daily locations of tagged ABT in each 1° latitude × 1° longitude bin was computed and used to identify hotspots of ABT presence throughout the Atlantic. Hotspots were defined as regions greater than 4° × 4° with more than the 90th percentile (=23.9) estimated locations in each 1° × 1° bin. Known bathymetric structures and oceanographic features were also considered when determining the boundaries of these hotspots (Table S1).

In the central Atlantic, ABT aggregated within the Newfoundland Basin (NB), whose hotspot boundaries were selected to enclose the 5000 m bathymetric contour north of 39 °N and south of 52 °N. The Coastal Ireland (CI) hotspot in the eastern Atlantic encompasses all ABT tagging locations in Irish shelf waters and extends west to the edge of the Irish continental shelf. It includes the Rockall Trough, a bathymetric feature bounded by a strongly sloping bottom topography. The southeast edge of the CI hotspot coincides with the northern edge of the Bay of Biscay (BoB) hotspot, demarcated by the midpoint of the English Channel. The eastern, southern, and western boundaries of the BoB hotspot were selected based on the boundaries defined on MarineRegions.org. The northern and southern edge of the West European Basin (WEB) hotspot coincide with the southwest edge of the Coastal Ireland hotspot and the southern edge of the Bay of Biscay, respectively. The western boundary of this hotspot encloses the 5000 m bathymetric contour west of the Bay of Biscay. The Mediterranean Sea (Med) was also included as a hotspot in the eastern Atlantic. Its extent was based on the boundaries defined on MarineRegions.org.

Residency of ABT in each of these hotspots varied by season. Total residency time (days) in each hotspot was calculated. Seasons were delineated by month: Fall includes September to November, Winter includes December to February, Spring includes March to May and Summer includes June to August.

2.4. Vertical diving behavior, habitat envelopes and mixed layer depth

After detachment from the fish, tags manufactured by Wildlife Computers, Inc. transmitted summaries of an individual's proportion of time spent in distinct depth and temperature bins. The number of depth or temperature bins, temporal resolution (i.e., 6-, 12- or 24-hour) and range (i.e., minimum and maximum depth/temperature) of bins differed amongst tag type and year of deployment. As such, all summaries were compiled to encompass the same depth and temperature bins and temporal resolution. Depth bins started at 0, 5, 10, 50, 100, 150, 200, 250, 300, 500, 700 and 1000 m. Temperature bins started at 0, 5, 10, 12, 14, 16, 18, 20, 22, 24, 26 and 28 °C. Time-at-depth and time-at-temperature were calculated for each fish in each hotspot, and then averaged across all individuals in each hotspot. The proportion of time spent at mesopelagic depths (i.e., greater than 200 m) was also calculated.

Tags manufactured by Wildlife Computers, Inc. also transmitted PAT-style Depth-Temperature (PDTs) profiles for 6, 12, or 24-h periods depending on tag programming. Each profile consists of the mean, maximum or minimum temperature values at 8 depths between the minimum and maximum occupied during the period. PSATFLEX tags manufactured by Lotek Wireless, Inc. transmitted partial time series of temperature and depth that were down sampled to create PDTs with 4 m resolution using the RchivalTag package in R (Bauer, 2022). Mean, maximum and minimum temperature values from PDTs were used to create vertical habitat envelopes of ABTs in each hotspot. Mixed layer depth (MLD; m) as well as the temperature at the MLD (°C) was calculated as described in Lawson et al. (2010) for all recovered tags as well as all PSATFLEX tags. Median sea surface temperature (SST) in each hotspot was calculated as the median temperature in the uppermost 5 m of the water column.

2.5. Satellite oceanographic data

Daily ADT between September 20, 2003 and September 30, 2021 was obtained from the SEALEVEL_GLO_PHY_L4_MY_008_047 delayed-time (i.e., reprocessed) product (https://doi.org/10.48670/moi-00148) distributed by Copernicus Marine Service. The zonal and meridian components of the geostrophic velocity anomalies were also obtained from this Level 4 product that combines data from 11 altimeter missions (i.e., Jason-3, Sentinel-3A, HY-2A, Saral/AltiKa, Cryosat-2, Jason-2, Jason-1, T/P, ENVISAT, GFO, and ERS1/2 satellites) to produce maps of eddy kinetic energy (EKE) with a spatial resolution of 0.25° × 0.25°.

Location, contours, amplitude and radius speed of anticyclonic and cyclonic eddies from September 20, 2003 to March 7, 2020 were acquired from the altimetric Mesoscale Eddy Trajectories Atlas delayed-time product (META3.1exp DT allsat, https://doi.org/10.24400/527896/a01-2021.001) distributed by AVISO +. Eddies from March 8, 2020 through September 30, 2021 were acquired from the near-real-time product META3.2exp NRT. These products use ADT from all available satellites at a given time to track eddies with lifetimes greater than 10 days using the algorithm described in Mason et al. (2014) and Pegliasco et al. (2022). Only the last instance of an eddy tracked over multiple days in a hotspot was used to compute summary statistics. Daily estimated locations of ABT were not linked to individual eddies due to the resolution of geolocation methods.

2.6. Statistical analysis

Differences in the percent time spent at mesopelagic depths and daily maximum depth (m) between each of the five hotspots and outside of these hotspots (i.e., between 20 and 70 °N and 80 °W and 40 °E) were assessed using the Kruskal-Wallis (KW) test. This test provides a non-parametric alternative to a one-way Analysis of Variance (ANOVA). Post-hoc comparisons were conducted using Tukey's honestly significant difference procedure at the 5% significance level. Percent time spent at mesopelagic depths and daily maximum depth were averaged within individuals in each hotspot before the KW test such that each fish contributed equally. The same statistical tests were used to evaluate differences between MLDs and temperatures at MLD as well as eddy properties between hotspots and outside of these hotspots. Correlations between ADT (m) and the percent time spent at mesopelagic depths and daily maximum depth, respectively, were tested using Spearman's rank correlation coefficient (ρ). The median value across all individuals within 1° × 1° latitude and longitude bins was taken prior to correlation. Non-parametric methods were used as the data had non-Gaussian distributions (Lilliefors test, p-values < 0.001). Median ($\tilde{x}$), median absolute deviation (MAD) and/or post-hoc p-values are reported in sections 3.2, 3.3 and 3.5 unless otherwise stated. KW χ^2 and p-values are reported in supplementary tables.

3. Results

We report the results from 51 ABT deployed from 2003 to 2020 off the coast of Ireland (Table 1). The curved fork length of the ABT used in

the analyses ranged from 170 to 240 cm (μ ± σ: 215 ± 15 cm). The mean (±σ) duration of deployments was 244 ± 103 days, ranging from 35 to 367 days post-release and generating over 4,887 light-based geolocations. Overall, straight line distances between deployment and pop-up locations ranged from 15 to 5795 km (μ ± σ: 1828 ± 1279 km). Six of the 51 tags were recovered, enabling the retrieval and analysis of the full archival record stored on the tag at high resolution.

3.1. Horizontal spatial distribution and seasonal residency patterns

The horizontal distribution of ABT in the northeast Atlantic post-release from Ireland is shown in Fig. 1. Over 78% of ABT remained in the eastern Atlantic throughout the entire tag deployment with only 11 ABT crossing the ICCAT 45 °W meridian management line (Fig. S1). Position estimates revealed that ABT occupied five hotspots in the central and eastern North Atlantic Ocean as well as the Med.

ABT were primarily located in the CI and BoB hotspots during the Fall months (Fig. 2a). Despite being tagged on the shelf of Donegal Bay or Courtmacsherry Bay from August through October, ABT remained in the CI hotspot for the second fewest number of days (μ ± σ: 20 ± 17 days; Fig. S2 and Table S2). Over 61% moved south to the foraging grounds in the BoB, many passing through the WEB, between 1 and 72 days after tagging. In both regions, ABT were often located along the edge of the continental shelf. Only 4 fish moved directly from the CI hotspot to the NB in the Fall months without entering the WEB or BoB.

During the Winter months, ABT were primarily located between 35 and 50 °N (Fig. 2b). During the transition from Fall to Winter, 75% of the remaining 48 tagged ABT moved from the BoB or WEB to the NB. In the NB, ABT were most often located within the topologically flat basin, away from the outer slope region. Two fish (5116032 and 5116042) travelled as far south as the Canary Islands in the eastern Atlantic and one fish (5103448) to the Bahamas in the western Atlantic (Fig. S5). A total of 40 tags collected data in the Spring. Most ABT returned to the eastern side of the Atlantic from the NB during this season, entering the WEB and BoB (Fig. 2c). Few fish were located within the CI hotspots. Two (5116031 and 5118054) traveled as far west as the Slope Sea off Massachusetts, United States (Fig. S5). Two (5116042 and 5120053) remained near the Canary Islands (Fig. S5).

Twenty-eight tags collected data during the Summer (Fig. 2d). Fourteen individuals entered the Med in May (CFL at entry μ ± σ: 227.3 ± 15.9 cm) and remained in this region through the end of the Summer. Tags that recorded potential spawning migrations were generally attached to the fish for 235 days post-release or more, with only two tags recording for less than this duration. Entry across the Strait of Gibraltar ranged from May 6 to 28, with a mean entry date of May 16 (Table S17). ABT remained in the Med between 18 and 135 days (μ ± σ: 53 ± 30 days; Table S2), with a mean exit date of July 7 (Table S17). Fish that entered the Med either spent fewer than 7 days ($n = 9$) or between 109 and 192 days ($n = 5$) in the BoB. Of the 14 ABT whose tags were operational in the Summer but did not enter the Med, two (5116031 and 5118057) were in the Slope Sea, three (5120065, 5120067 and 5120069) remained in the NB and one (5116036) remained in the WEB (Fig. S5). One (5120061) traveled east to the BB from the WEB and another (5116032) traveled north from the WEB to the Faroe Islands (63.4578 °N, −3.9249 °W) (Fig. S5). Three (5120051, 5120053 and 5120054) ABT were initially tagged in August while another 3 (5116038, 5118056 and 5120072) only had 2 daily geolocations or less during the Summer (Fig. S5).

3.2. Vertical diving behavior

Across all five hotspots, ABT spent the majority of their time in the top 50 m (72.0 to 83.4%). The highest percentage of time was spent at depths between 0 and 5 m (28.1 to 42.5%), and 10 to 50 m (19.8 to 37.3%) (Fig. 3). Comparatively little time was spent at mesopelagic depths (i.e., greater than 200 m) (Fig. 4a and Table S3). Though, significantly higher time was spent at mesopelagic depths in the WEB and NB (4.8 ± 1.9 % for WEB and 3.0 ± 1.3 % for NB) than in the CI hotspot and BoB (0.2 ± 0.2 % for CI and 1.2 ± 0.9 % for BoB) (p-values < 0.001 except for BoB vs. NB p-value = 0.04; Table S4). The median daily maximum depth was 265.9 ± 61.1 m in the WEB and 232.2 ± 51.9 m in the NB (Fig. 5a and Table S5), with ABT reaching 1500 m in some instances in both hotspots. In these hotspots, ADT was positively correlated with both the percent time at mesopelagic depths ($\rho = 0.35$, p-value < 0.001 for WEB, $\rho = 0.25$, p-value = 0.002 for NB; Fig. 4b) and daily maximum depth ($\rho = 0.43$ for WEB, $\rho = 0.28$ for NB, p-values < 0.001; Fig. 5b) (Table 2). Additionally, the daily maximum depth for ABT was routinely greater than 300 m on the western side of the WEB and in the southwest corner of the NB (Fig. 5c).

Conversely, about 73% of average daily maximum depths for each individual fish were shallower than 200 m in the CI hotspot (Fig. 3a). However, ABT routinely dove deeper than 300 m and spent more than 5% of their time at mesopelagic depths in the northeast corner of the hotspot (Fig. 4c & 5c). Overall, ADT was negatively correlated with both percent time at mesopelagic depths ($\rho = -0.52$, p-value < 0.001; Fig. 4b) and median daily maximum depth ($\rho = -0.57$, p-value < 0.001; Fig. 5b) in this hotspot (Table 2). There was no significant relationship between ADT and either dive metric in the BoB or the Med (Fig. 4b & 5b and Table 2). Though, increased time at mesopelagic depths and deeper daily maximum depths occurred near the entrance of the Med (Fig. 4c & 5c).

Behavior outside of the five hotspots was comparable to that in the WEB and NB (69.8 ± 6.6% at depths shallower than 50 m; Fig. 3f), with similar use of mesopelagic depths (3.6 ± 2.1%; Fig. 4a) and median daily maximum depth (279.4 ± 50.8 m; Fig. 5a). Both dive metrics were positively correlated with ADT ($\rho = 0.09$, p-value = 0.03 for % time in mesopelagic, $\rho = 0.24$, p-value < 0.001 for daily maximum depth; Fig. 4b & 5b and Table 2). Median daily maximum depths greater than 400 m and greater than 10% time spent at mesopelagic depths occurred at various locations including southwest of the Azores, along the Faraday and Maxwell Fracture Zones (MFZ) as well as at the entrance of the Med in the Gulf of Cadiz and on the Seine Abyssal Plain (Fig. 4c & 5c).

3.3. Habitat envelopes

ABT in the NB occupied waters with temperatures between 16 and 18 °C for 57.1 ± 16.1% of the time (Fig. S3d). The median SST in this hotspot was 16.8 ± 1.1 °C. Water temperatures of 16 °C were experienced by ABT down to 648 m, while temperatures of 18 °C were experienced down to 544 m (Fig. 6d). Additionally, the deepest MLDs were measured in the NB (122 ± 57 m; Table 3). However, there was no significance difference in the temperature at the MLD in the NB to that in the BoB (13.8 ± 1.4 °C for BoB vs. 15.0 ± 1.8 °C for NB, p-value = 0.99; Tables 3 & S8) despite significantly shallower MLDs in the BoB (60 ± 20 m for BoB, p-value < 0.001; Tables 3 & S7).

Deep MLDs were also measured in the WEB (90 ± 36 m; Tables 3). Here, the median temperature at the MLD was similar to that in the CI hotspot (13.7 ± 0.4 °C for CI vs. 13.2 ± 1.0 °C for WEB, p-value = 1.00; Tables 3 & S8). However, MLDs in the CI hotspot were significantly shallower (43 ± 17 m for CI, p-value < 0.001 vs. WEB; Tables 3 & S7). ABT in these hotspots spent a median 30.5 ± 16.9% and 38.3 ± 29.4%, respectively, in waters with temperatures between 12 and 14 °C (Fig. S3a & c). Overall, thermal habitat envelopes for the CI hotspot and WEB had similar shapes to that in the BoB (Fig. 6a-c). The MLDs in the CI hotspot were not significantly different from those in the BoB (p-value = 0.18; Table S7). However, ABT in the BoB spent most of their time in waters with temperatures between 16 and 18 °C (23.3 ± 12.3 %; Fig. S3b) and temperatures below 50 m were about 1.4 °C warmer in the BoB than in the CI hotspot. Additionally, the median SST was slightly higher in the BoB (14.6 ± 2.0 °C) than in the CI and WEB (13.6 ± 1.2 °C for CI, 13.2 ± 1.2 °C for WEB).

ABT in the Med experienced much warmer waters and a smaller temperature range than the other hotspots (Fig. 3e), spending 73.5 ± 10.5% of their time in waters with temperatures greater than 18 °C (Fig. S3e). About 24.0 ± 11.4% of their time was spent in waters with temperatures between 22 and 26 °C (Fig. S3e), a range that encompasses the 23.5 to 25 °C waters that are considered ideal for ABT spawning in the Med (Alemany et al., 2010; García et al., 2005). Additionally, the highest SSTs (21.9 ± 2.1 °C) as well as the shallowest MLDs (15 ± 2 m) and warmest temperatures at the MLD (20.4 ± 1.5 °C) occurred in this hotspot (Table 3). Median MLDs and temperatures at the MLD within the hotspots were significantly different than all other hotspots as well as outside the five hotspots (p-values = 0.00; Tables S7 & S8).

ABT spent on average (±σ) 27.8 ± 20.5% of their time traveling between the five hotspots (Fig. S2), where the median SST was 16.3 ± 1.7 °C. During this time, fish occupied waters of 14 to 16 °C for 27.5 ± 10.9% of the time (Fig. S3f). The MLDs (68 ± 40 m) were significantly shallower than MLDs in the NB and WEB (p-value < 0.001 vs. NB, 0.004 vs. WEB), and significantly deeper than in the CI hotspot, BoB and Med (p-value < 0.001 vs. CI, 0.03 vs. BoB and 0.00 vs. Med) (Tables 3 & S7). Temperatures at the MLD (15.4 ± 1.2 °C) were significantly colder than those in the NB and Med (p-value < 0.001 vs. NB, 0.00 vs. Med), and significantly warmer than those in the CI hotspot, BoB and WEB (p-value = 0.00 vs. CI & WEB, < 0.001 vs. BoB) (Tables 3 & S8).

3.4. Example tracks and time series of ABT that traveled to the Mediterranean Sea

Figs. 7 and 8 show two example tracks and time series of ABT tagged off the coast of Ireland that eventually entered the Med. ABT 5116034 (CFL at tagging = 220 cm) immediately traveled south after it was tagged on the shelf of Donegal Bay in the CI hotspot in October 2016, reaching the BoB by traveling through the WEB in 16 days (Fig. 7b and Table S2). Unlike the other tagged ABT shown in Fig. 8, this fish spent approximately 81% of the tag's 238-day deployment in the BoB and never traveled to the NB hotspot. In the BoB, the fish experienced gradually colder mean (±σ) temperatures from 16.2 ± 1.2 °C in November 2016 to 11.8 ± 0.6 °C in February 2017 (Fig. 7a). Mean (±σ) temperatures in this hotspot increased to 12.8 ± 0.4 °C in early May 2017, at which time the fish exited the BoB and traveled through the WEB to reach the Med. The ABT crossed the Strait of Gibraltar on May 19, 2017, at an estimated CFL of 225.6 cm (Table S17). During its 18 days in the Med, this fish experienced temperatures ranging from 13.4 to 24.5 °C (μ ± σ: 18.7 ± 2.7 °C). Unfortunately, the ABT was potentially captured and penned around June 5, 2017, in the Med. Two other fish that traveled to the Med (ABT 5116035 and 5120071) had similar tracks (Fig. S5). Each spent over 50% of their time in the BoB and no days in the NB.

ABT 5116043 (CFL at tagging = 234 cm) is the only recovered tag that visited all five hotspots during its 309-day deployment (Fig. 8 and Table S2). Seven days after it was tagged on the shelf of Donegal Bay in the CI hotspot in October 2016, the fish entered the WEB briefly before heading west towards the NB. From December to March when the fish was in the NB, it experienced a mean temperature of 16 °C throughout the water column and frequently dove into the mesopelagic up to depths of 960 m (Fig. 8a). In March 2017, the fish traveled back across the Atlantic to the Med, crossing the Strait of Gibraltar on May 21, 2017, at an estimated CFL of 238.4 cm (Table S17). After 47 days in the Med where it occupied waters as warm as 26.2 °C, it exited and headed north, passing through the WEB and BoB before returning to the CI. Waters in these regions were highly stratified, with a mean water temperature of 14.5 °C above and of 11.1 °C below 50 m. The fish nearly completed a round trip migration, returning to a region only 180 km south of its original tagging location. Four other ABT (ABT 5117023, 5118058, 5118061 and 5120057) had similar tracks (Fig. S5). Each spent between 17 and 28% of their time in the NB and less than 2% of their time in the BoB.

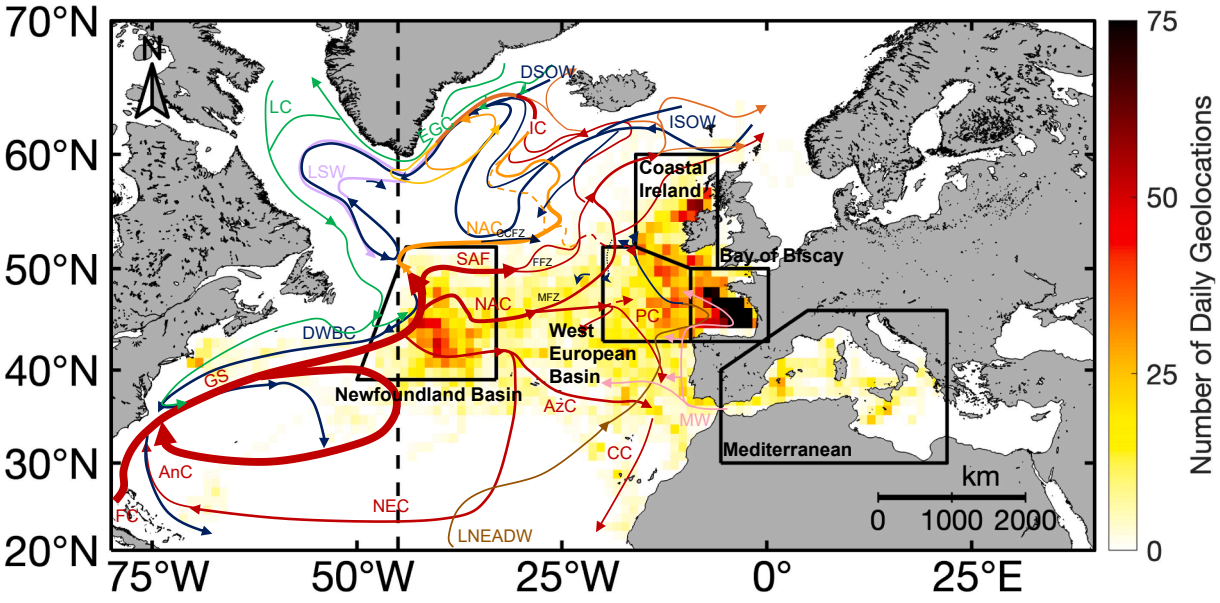

Fig. 1. Number of daily geolocations of 51 PSAT-tagged ABT released off Ireland within 1° × 1° latitude and longitude bins with schematic diagram of the North Atlantic circulation overlayed, adapted from Carracedo et al. (2021) and Daniault et al. (2016). Boundaries of North Atlantic and Mediterranean hotspots are outlined in solid black. The International Commission for the Conservation of Atlantic Tunas 45 °W meridian management line is also shown (dashed black line). Labeled water masses and currents include Antilles Current (AnC, red line), Azores Current (AzC, red line), Canary Current (CC, red line), Deep Western Boundary Current (DWBC, blue line), Denmark Strait Overflow Water (DSOW, blue line), East-Greenland Current (ECG, green line), Florida Current (FC, red line), Gulf Stream (GS, red line), Iceland–Scotland Overflow Water (ISOW, blue line), Irminger Current (IC, orange line), Labrador Current (LC, green line), Labrador Sea Water (LSW, purple line), Lower North East Atlantic Deep Water (LNEADW, brown line), Mediterranean Water (MW, pink line), North Atlantic Current (NAC, orange and red lines), North Equatorial Current (NEC, red line), Portugal Current (PC, red line) and Subarctic Front (SAF, red line). The Charlie–Gibbs Fracture Zone (CGFZ), Faraday Fracture Zone (FFZ) and Maxwell Fracture Zone (MFZ) are also noted. See Fig. S1 in the Supplementary Information for actual tracks.

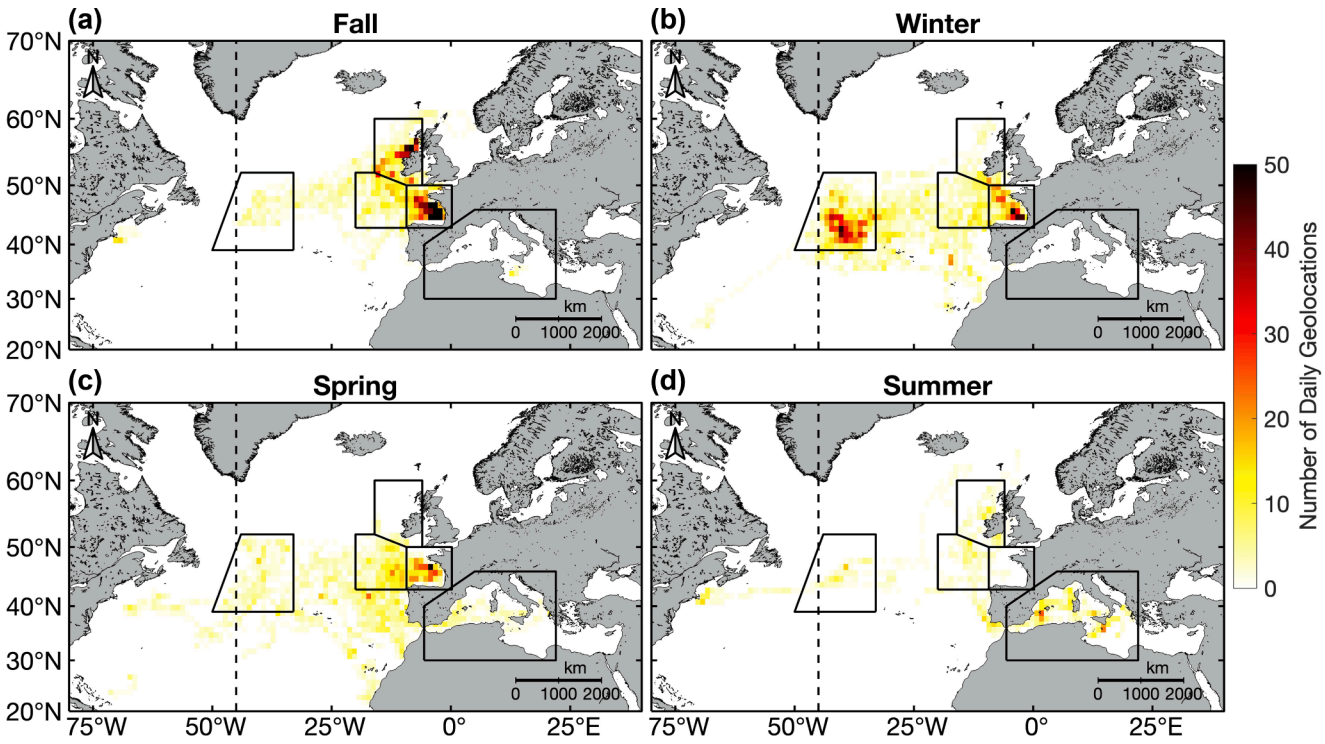

Fig. 2. Number of daily geolocations within 1° × 1° latitude and longitude bins in (a) Fall (n = 51), (b) Winter (n = 48), (c) Spring (n = 40) and (d) Summer (n = 28). Boundaries of hotspots are outlined in black. The International Commission for the Conservation of Atlantic Tunas 45 °W meridian management line is also shown (dashed black line).

3.5. Properties of eddies in hotspots

Overall, the NB was the most energetic hotspot and had the highest number of unique eddies (n = 542 ACEs, n = 599 CEs; Table 4). Properties of eddies of both polarities in this hotspot were significantly different than eddies outside of the five hotspots (Fig. 9 and Tables 4 & S9–16). Eddies were larger in eddy speed radius (33.2 ± 6.0 km vs. 32.0 ± 5.8 km for ACEs, 33.0 ± 5.5 km vs. 32.0 ± 5.7 km for CEs, p-values < 0.001) and amplitude (3.4 ± 1.6 cm vs. 1.3 ± 0.6 cm for ACEs, 4.1 ± 2.0 cm vs. 1.3 ± 0.6 cm for CEs, p-values = 0.00), had a faster average axial speed (20.3 ± 6.6 cm/s vs. 8.1 ± 2.8 cm/s for ACEs, 22.5 ± 7.3 cm/s vs. 8.2 ± 2.7 cm/s for CEs, p-values = 0.00), and had a longer lifetime (3.8 ± 2.2 weeks vs. 3.3 ± 1.9 weeks, p-value = 0.01 for ACEs, 3.9 ± 2.6 weeks vs. 3.3 ± 1.9 weeks, p-value < 0.001 for CEs). Additionally, both ACEs and CEs in the NB were also significantly larger in amplitude and faster in average axial speed than eddies in the other four hotspots (p-values = 0.00; Fig. 9b-c & f-g and Tables S10–11 & S14–15). Lifetime of eddies of both polarities in the NB were similar to those in the WEB (p-value = 0.99 for ACEs, 0.94 for CEs) and Med (p-values = 1.00) (Fig. 9d & h and Tables S12 & S16). Mean EKE was higher on the west side of the basin on days when ABT were present (Fig. 10b), especially northeast and southwest of the region between 39 and 48 °W and 40 to 43 °N, where the mean ADT was strongly positive (Fig. 10c).

Three properties of CEs in the WEB were significantly different than those of CEs outside of the five hotspots (Fig. 9e & g-h and Tables 4, S13 & S15–16). Cyclones had larger radii (32.4 ± 5.4 km, p-value = 0.03), and longer lifetimes (4.4 ± 3.0 weeks, p-value < 0.001) but were slower (7.2 ± 2.5 cm/s, p-value < 0.001). Anticyclones in the WEB had significantly longer lifetimes (4.3 ± 2.9 weeks, p-value = 0.002) and slower speeds (7 ± 2.3 cm/s, p-value < 0.001) than ACEs outside of the five hotspots but were not significantly different in radius (32.7 ± 5.8 km, p-value = 0.06) or amplitude (1.3 ± 0.6 cm, p-value = 1.00) (Fig. 9a-d and Tables 4 & S9–12). The steep continental shelf that extends diagonally from the northwest corner to the center of the WEB as well as across the WEB at 45 °N created a region with higher EKE in the west and lower EKE in the east of the basin (Fig. 11a); though the mean ADT was slightly positive throughout (Fig. 11b).

Eddies of both polarities in the CI hotspot were significantly slower (6.5 ± 1.9 cm/s for ACEs, 6 ± 2.0 cm/s for CEs, p-values < 0.001) and had significantly shorter lifetimes (2.4 ± 1.6 weeks, p-value < 0.001 for ACEs, 2.7 ± 1.4 weeks, p-value = 0.001 for CEs) than eddies outside of the five hotspots (Fig. 9c-d & g-h and Tables 4, S11–12 & S15–16). However, the radius (31.6 ± 5.7 km, p-value = 1.00 for ACEs, 31.4 ± 5.4 km, p-value = 0.94 for CEs) and amplitude (1.2 ± 0.6 cm, p-value = 0.98 for ACEs, 1.3 ± 0.6 cm, p-value = 1.00 for CEs) of both ACEs and CEs were not significantly different from eddies outside of the five hotspots (Fig. 9a-b & e-f and Tables 4, S9–10 & S13–14). Additionally, the radius, amplitude and speed of ACEs in the CI hotspot were similar to those in the WEB (p-value = 0.25 for L_s, 1.00 for A and 0.64 for U_{avg}; Tables S9–11) while the amplitude of CEs in the CI hotspot were similar to those in both the WEB and Med (p-value = 0.79 for WEB, 0.73 for Med; Table S14). Within the Rockall Trough, higher mean EKE, and strongly positive mean ADT were observed on days when ABT were in the CI hotspot (Fig. 11c & d).

The lowest number of unique eddies (n = 176 ACEs, n = 222 CEs; Table 4) occurred in the BoB. Eddies in this hotspot were the smallest in amplitude (0.9 ± 0.3 cm for ACEs and CEs, p-values < 0.001 except p-values = 0.00 vs. NB) and slowest (4.2 ± 1.1 cm/s for ACEs, 4.5 ± 1.2 cm/s for CEs, p-values = 0.00 except p-values < 0.001 vs. WEB) (Fig. 9b-c & f-g and Tables 4, S10–11 & S14–15). These eddies also had significantly shorter lifetimes than eddies of both polarity in the other four hotspots and outside of the five hotspots (2.6 ± 1.1 weeks for ACEs, 2 ± 0.7 weeks for CEs, p-values < 0.001; Fig. 9d & h and Tables 4, S12 & S16), except ACEs in the CI hotspot, which had longer lifetimes (p-value < 0.001). While eddies of both polarities were significantly larger in radius than eddies outside of the five hotspots (36.5 ± 6.2 km for ACEs, 32.4 ± 5.5 km for CEs, p-values < 0.001), there was no difference in radius to eddies in the NB and Med (p-value = 0.24 vs. NB, 0.99 vs. Med

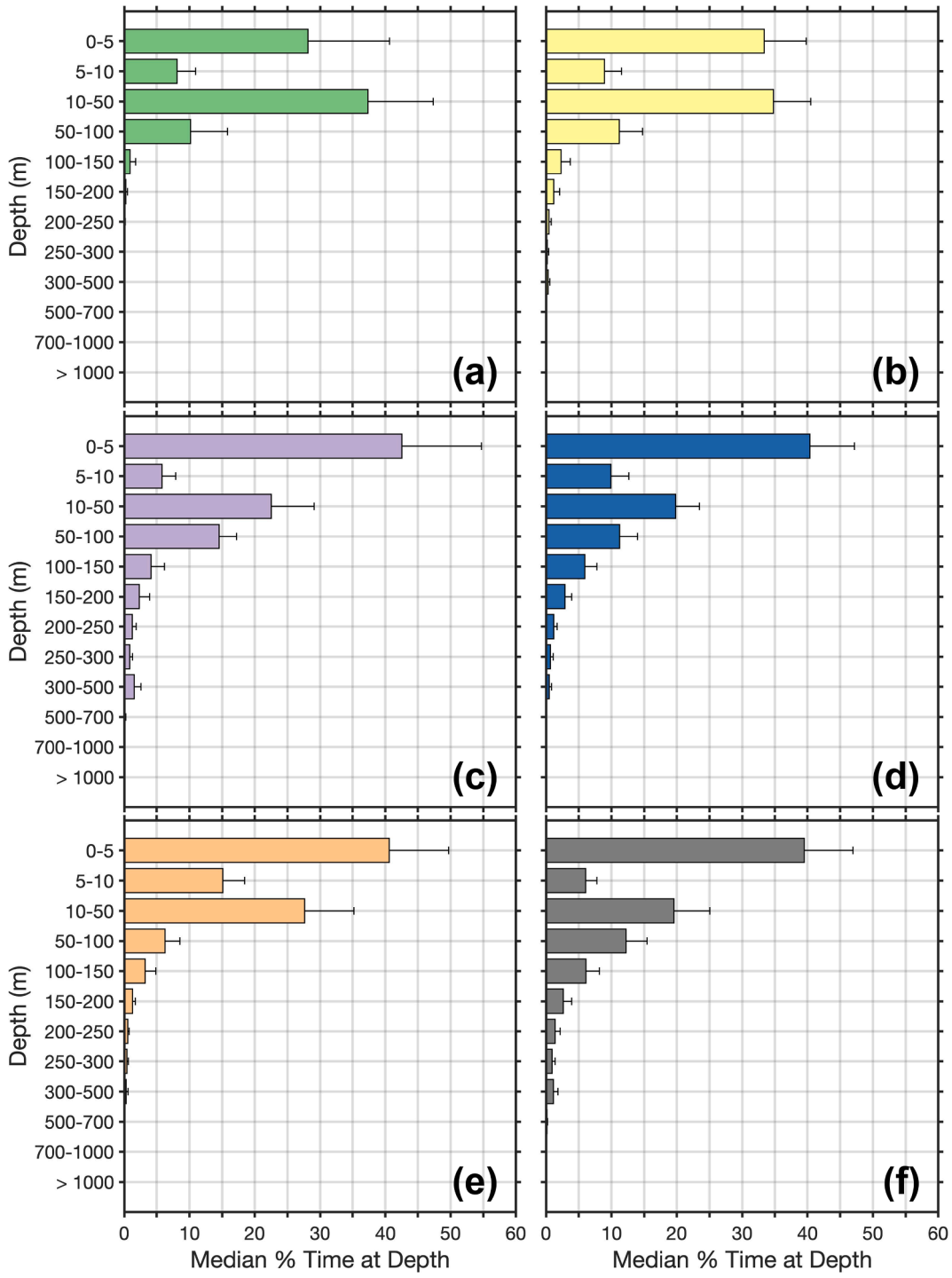

Fig. 3. Median percent time at depth (m) histograms for all Atlantic bluefin tuna in the (a) Coastal Ireland, (b) Bay of Biscay, (c) West European Basin, (d) Newfoundland Basin and (e) Mediterranean Sea hotspot as well as (f) outside of these hotspots. Error bars represent median absolute deviation.

for ACEs, 0.40 vs. NB, 0.56 vs. Med for CEs) (Tables 4, S9 & S13). Further, the steep continental slope in the BoB appeared to trap eddies of both polarities between 2 and 4 °W and 43.5 to 45 °N (Fig. S4g & h). However, this did not correspond to elevated mean EKE or mean ADT (Fig. 11e & f).

In the Med, eddies of both polarities had significantly larger radii (36.7 ± 6.8 km for ACEs, 36.6 ± 5.8 km for CEs, p-values < 0.001) than eddies outside of the five hotspots (Fig. 9a & e and Tables 4, S9 & S13). However, both ACEs and CEs in the Med had similar speeds (8.2 ± 2.6 cm/s, p-value = 0.80 for ACEs, 8 ± 2.4 cm/s, p-value = 0.89 for CEs) and lifetimes (3.9 ± 2.4 weeks for ACEs and CEs, p-value = 0.24 for ACEs, 0.06 for CEs) to eddies outside of the five hotspots (Tables 4, S11–12 & S15–16). Amplitudes of ACEs were significantly different than eddies in the other four hotspots as well as outside of the five hotspots (1.5 ± 0.8 cm, p-values = 0.00 vs. NB, 0.01 vs. WEB, 0.005 vs. CI, < 0.001 vs. BoB & Outside; Fig. 9b and Tables 4 & S10). Amplitudes of CEs were similar to eddies in the WEB and outside of the five hotspots (1.4 ± 0.7 cm, p-values = 1.00 vs. WEB, 0.22 vs. Outside; Fig. 9f and Tables 4 & S14). Positive mean ADT and higher mean EKE occurred in the southern half of the Med while negative mean ADT and lower mean EKE occurred in

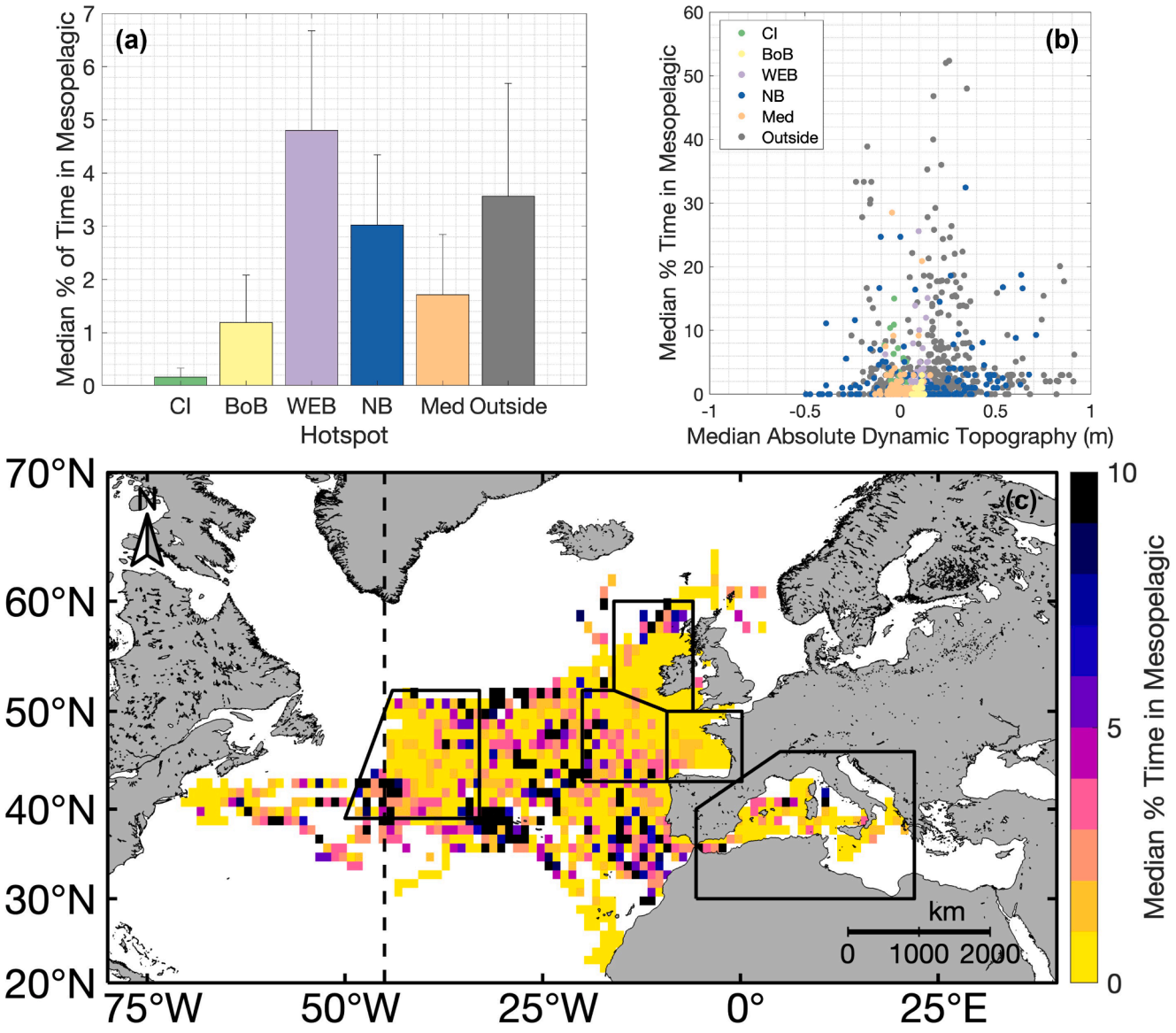

Fig. 4. (a) Median percent time at mesopelagic depths (i.e., below 200 m) in the Coastal Ireland (CI; green), Bay of Biscay (BoB; yellow), West European Basin (WEB; purple), Newfoundland Basin (NB; blue) and Mediterranean Sea (Med; orange) hotspots as well as outside of these hotspots (grey). Error bars represent median absolute deviation. (b) Relationship between median absolute dynamic topography (m) and median percent time at mesopelagic depths. Each dot represents a 1° × 1° latitude and longitude bin. Dots are colored by hotspot. (c) Median percent time at mesopelagic depths within 1° × 1° latitude and longitude bins. Boundaries of hotspots are outlined in solid black. The International Commission for the Conservation of Atlantic Tunas 45 °W meridian management line is also shown (dashed black line). Colorbar is cut to a maximum of 10%.

the northern half (Fig. 11g & h). Overall, the highest mean ADT and mean EKE was at the entrance of the Med.

4. Discussion

Electronic tagging of ABT has provided a wealth of data that have shaped our understanding of their movements and migrations throughout the Atlantic basin. However, compared to the western Atlantic, less is known about the annual movement patterns of large ABT in the eastern Atlantic as fewer long duration tracks have been collected, particularly for ABT tagged outside the Med. Here, we present a dataset of ABT tagged off the coast of Ireland between 2003 and 2020 with long tag retention times (μ ± σ: 244 ± 103 days). Fish in this area are presumed to originate primarily from the Med spawning ground. Previous studies on the spatial movements of this stock of ABT have primarily been based on smaller fish tagged within the Med (e.g., Cermeño et al., 2015; De Metrio et al., 2005, 2002, 2001; Fromentin and Lopuszanski, 2014; Quílez-Badia et al., 2015; Tudela et al., 2011), which may represent a distinct subpopulation from the fish tagged in this study. Our current and prior reported efforts in Ireland (Horton et al., 2020; Stokesbury et al., 2007) in addition to recent efforts by Aarestrup et al., (2022) now provide an opportunity to fully examine the movements of large ABT in the NAO, identifying how they interact with the currents and eddies as well as the timing of entry to the Med for spawning.

4.1. Spatial distribution relative to currents in the North Atlantic Ocean

The large-scale circulation in the NAO plays a major role in shaping the spatial distribution of ABT in the Atlantic (Fig. 1). ABT tagged off Ireland in the Fall were primarily located within a region bounded by two eastward flowing currents that originate from a bifurcation of the Gulf Stream at the Grand Banks of Newfoundland (e.g., Rossby, 1996). The northern extent of ABT west of 20 °W closely aligned with the central branch of the North Atlantic Current (NAC). The NAC is a warm

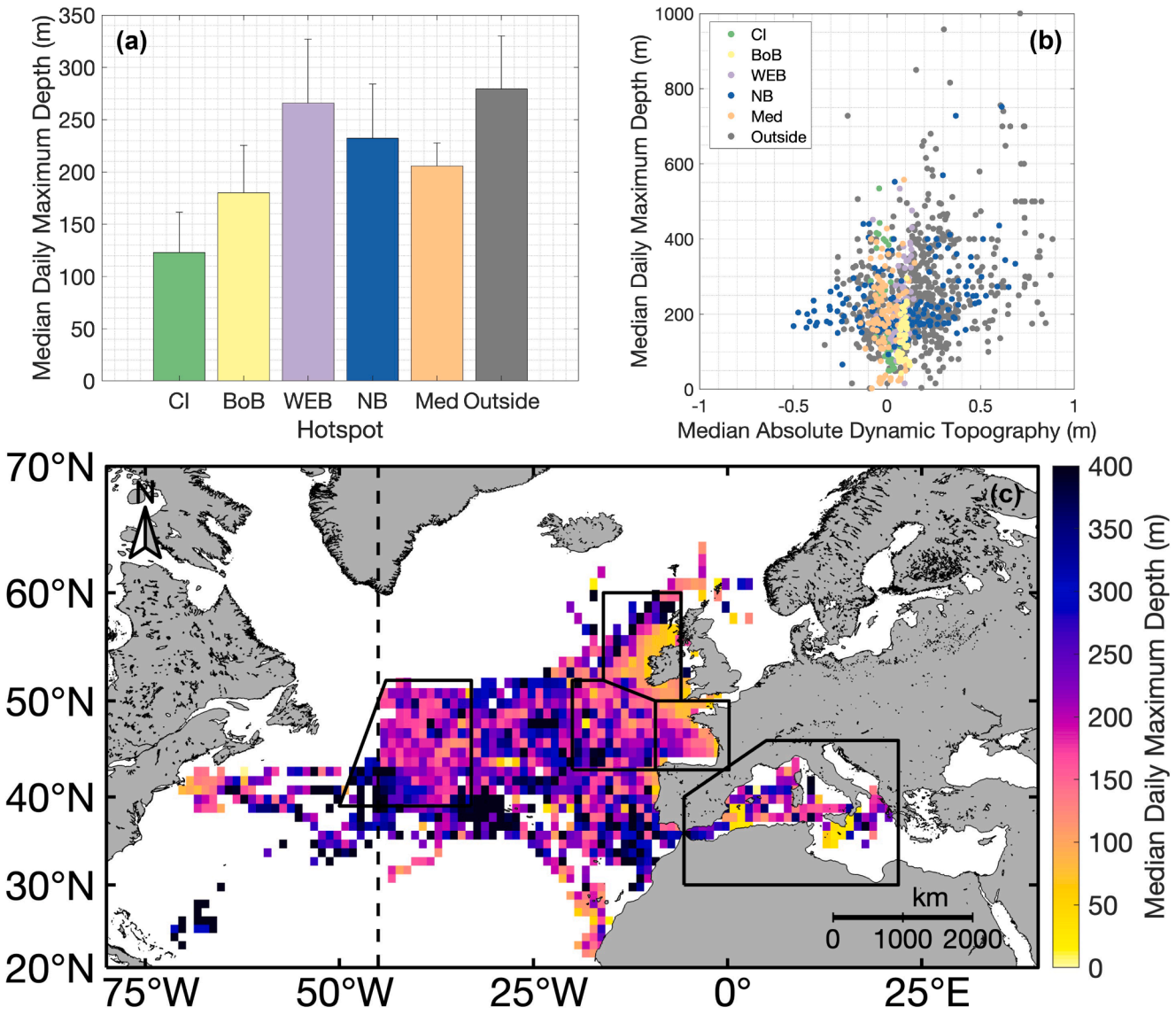

Fig. 5. (a) Median daily maximum depth (m) in hotspots (as in Fig. 4) as well as outside of these hotspots. Error bars represent median absolute deviation. (b) Relationship between median absolute dynamic topography (m) and median daily maximum depth (m). Each dot represents a 1° × 1° latitude and longitude bin. Dots are colored by hotspot. (c) Median daily maximum depth (m) within 1° × 1° latitude and longitude bins. Boundaries of hotspots are outlined in solid black. The International Commission for the Conservation of Atlantic Tunas 45 °W meridian management line is also shown (dashed black line). Colorbar is cut to a maximum of 400 m.

Table 2
Spearman's rank correlation coefficients (ρ) for correlations between median absolute dynamic topography (m) and median percent time in the mesopelagic and median daily maximum diving depth (m), respectively, within 1° × 1° latitude and longitude bins in each hotspot (CI: Coastal Ireland, BoB: Bay of Biscay, WEB: West European Basin, NB: Newfoundland Basin, Med: Mediterranean Sea), outside of these hotspots and throughout all areas. Bolded values indicate a significant difference at the 5% level.

	% Time in Mesopelagic		Daily Maximum Diving Depth	
	ρ	*p*-value	ρ	*p*-value
CI	**−0.52**	**< 0.001**	**−0.57**	**< 0.001**
BoB	0.22	0.17	0.25	0.10
WEB	**0.35**	**< 0.001**	**0.43**	**< 0.001**
NB	**0.25**	**0.002**	**0.28**	**< 0.001**
Med	−0.04	0.70	0.00	0.97
Outside	**0.09**	**0.03**	**0.24**	**< 0.001**
All	**0.18**	**< 0.001**	**0.27**	**< 0.001**

current that flows northeastward across the Atlantic basin in several branches that are topographically steered and is the upper limb of the Atlantic Meridional Overturning Circulation (AMOC) (Daniault et al., 2016; García-Ibáñez et al., 2015). The central branch, also known as the Subarctic Front, corresponds to a sharp salinity front that separates the Subpolar Gyre from the Subtropical Gyre and is quasi-locked to the Faraday Fracture Zone near 50-51°N (Daniault et al., 2016; Roessler et al., 2015; Stendardo et al., 2020, 2016). Bluefin tuna in other ocean basins are also closely associated with frontal zones. In the Pacific, the northern extent of Pacific bluefin tuna (*Thunnus orientalis*) closely aligns with the Subarctic Front (Fujioka et al., 2018; Kitagawa et al., 2009). Southern bluefin tuna (*Thunnus maccoyii*) in the Indian Ocean are often found north of the Subantarctic Front (Bestley et al., 2009).

East of 20 °W, the northern extent of the ABT tagged off the coast of Ireland was delineated by northeastward flow towards the Rockall Trough off the coast of Ireland that originates from a secondary split of the southern branch of the NAC at the MFZ near 48 °N (Daniault et al., 2016). The Azores Current, which flows southeastward until it crosses

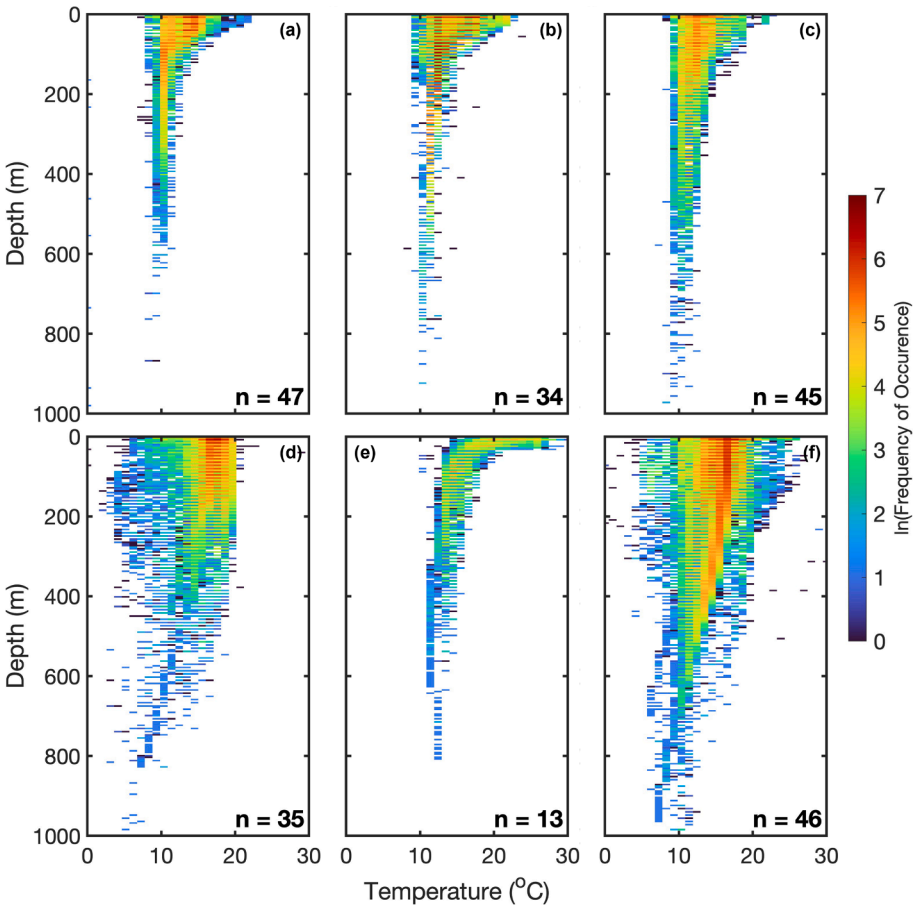

Fig. 6. Habitat envelopes for each of the five hotspots: (a) Costal Ireland, (b) Bay of Biscay, (c) West European Basin, (d) Newfoundland Basin and (e) Mediterranean Sea. Habitat envelope for all temperature-depth data collected (f) outside of the five hotspot is also shown.

Table 3
Median (± median absolute deviation) mixed layer depth (MLD; m) and median (± median absolute deviation) temperature at the MLD (°C) in each hotspot with number of profiles considered from all recovered tags as well as all PSATFLEX tags. All median values for both MLD and temperature at MLD are significantly different from outside of the hotspots at the 5% level. *p*-values are listed in Table S7 and S8.

	Mixed Layer Depth (MLD; m)	Temperature at MLD (°C)	*n*
CI	43 ± 17	13.7 ± 0.4	230
BoB	60 ± 20	13.8 ± 1.4	405
WEB	90 ± 36	13.2 ± 1.0	267
NB	122 ± 57	15.0 ± 1.8	233
Med	15 ± 2	20.4 ± 1.5	653
Outside	68 ± 40	15.4 ± 1.2	944

the Mid-Atlantic Ridge, delineated the southern extent of ABT (Klein and Siedler, 1989). This finding suggests that the distribution of large ABT tagged off Ireland might be directly related to the presence of the warm and salty subtropical water transported across the Atlantic basin by these currents and their branches. Previous studies that have tracked ABT from Irish and Scandinavian waters also observed a similar spatial extent for large ABT in the NAO (Aarestrup et al., 2022; Horton et al., 2020; Stokesbury et al., 2007). We found no relationship between the spatial distribution of ABT and smaller-scale SST fronts as described in Belkin et al., (2009) and Mauzole (2022). However, this could be due to the coarser resolution of currently available geolocation methods compared to satellite imagery from which these SST frontal maps are derived.

4.2. *Newfoundland Basin and West European Basin*

We identified five hotspots of ABT presence in the NAO largely based on the total number of daily estimated locations of tagged ABT in each 1° latitude × 1° longitude bin (Fig. 1). The NB was the most distinct hotspot both oceanographically and behaviorally. Seventy-one percent of ABT tagged in this study visited this North Atlantic hotspot, primarily in the Winter. Previous studies have shown that some small ABT tagged in the BoB also traveled to the NB in the Winter (Arregui et al., 2018). Additionally, ABT tagged off the coast of North Carolina, USA also spent extended time in the NB, but their presence peaked during the Summer (Walli et al., 2009).

The NB is a region of active eddy formation with intense mesoscale eddy activity. On average, the eddies in the NB when ABT were present were the largest and fastest of any hotspot (Fig. 9 and Table 4). These eddies are a major component of the NAC, whose flow has also been described as a train of long-lasting, slow-moving, highly energetic, mesoscale eddies instead of branches (Heywood et al., 1994; Krauss, 1986; Read et al., 2010; Richardson, 1993). Additionally, we found that a deep isothermal layer extended from the surface to nearly 120 m in the NB, with temperatures of over 18 °C down to almost 545 m (Fig. 6d and Table 3). Previous studies showed that this warm water in the NB is also relatively oxygen-rich, likely due to the "leakiness" of the southward-flowing deep limb of AMOC carrying cold, more recently aerated waters from the Labrador Sea into the NB (Racapé et al., 2019; Rhein et al., 2017; Richardson, 1993; Solodoch et al., 2020; Stendardo and Gruber, 2012). This warm, oxygen-rich water might expand the vertical habitat that ABT can occupy, minimizing both metabolic maintenance and digestive expenditures, and maximizing foraging opportunities. This

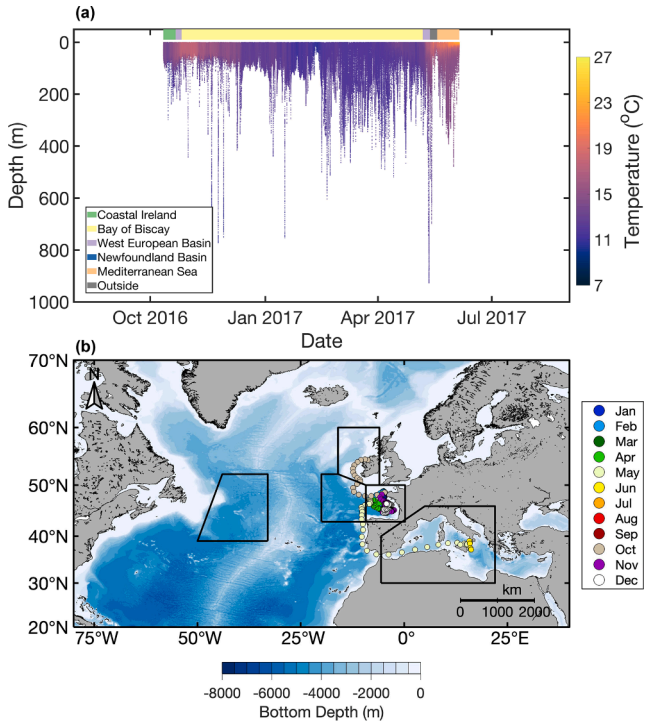

Fig. 7. (a) Archived depth and temperature time series and (b) daily geolocations for Atlantic bluefin tuna #5116034 tagged off the coast of Ireland. Depth traces are shaded by temperature and labeled horizontal color denotes the hotspot in which the ABT is located. Daily geolocations are colored by month. Boundaries of hotspots are outlined in solid black.

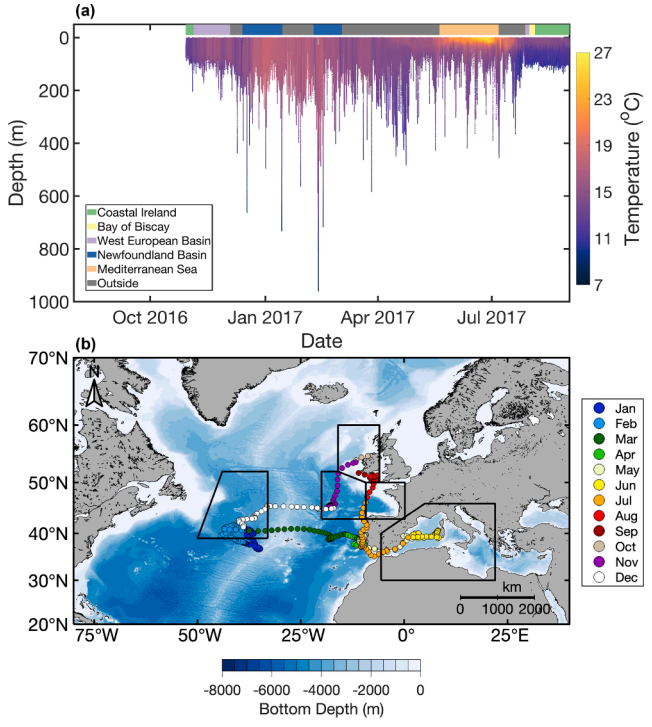

Fig. 8. (a) Archived depth and time series and (b) daily geolocations for Atlantic bluefin tuna #5116043 tagged off the coast of Ireland. Depth traces are shaded by temperature and labeled horizontal color denotes the hotspot in which the ABT is located. Daily geolocations are colored by month. Boundaries of hotspots are outlined in solid black.

also aligns with previous ABT studies that have found that ABT dive deeper in water columns with deeper mixed layer depths (Lawson et al., 2010; Wilson and Block, 2009; Wilson et al., 2005).

ABT tagged in this study often dove to depths greater than 400 m (Fig. 5c) and spent increased time at mesopelagic depths in the southwest corner of the NB (Fig. 4c), where the mean ADT is strongly positive (Fig. 10c). This is the climatologic signature of the Mann Eddy, a long-lived, quasi-stationary, mesoscale anticyclone trapped by the bowl-like topography of the basin (Mann, 1967; Solodoch et al., 2021). This co-occurrence drives the strong, positive correlations between ADT and daily maximum depth as well as time spent at mesopelagic depths, respectively, within the NB (Fig. 4b & 5b and Table 2). However, the area within the NB with the highest number of daily estimated locations occurred northeast of the Mann Eddy and southwest of the Newfoundland Basin Recirculation Gyre (NBRG) (Fig. 10a). The NBRG is where the central branch of the NAC flows southward, recirculating anticyclonically (i.e., clockwise) in the basin and creating a field of semi-permanent eddies (Bower et al., 2009; Caniaux et al., 2001; Gary et al., 2011; Mertens et al., 2014; Richardson, 1993). Deep diving and increased time at mesopelagic depths also occurred near this southward split of the central branch.

The diving behavior of ABT in the WEB was similar to that in the NB (Figs. 3, 4 & 5). In the southwest corner of the WEB, the daily maximum depth of ABT often surpassed 400 m (Fig. 5c) and ABT spent over 5% of their time at mesopelagic depths (Fig. 4c). The circulation in this corner of the WEB is like the circulation in the NBRG. The southeastward flow in the WEB originates from a secondary split of the southern branch of the NAC at the MFZ and recirculates anticyclonically in the basin (Bersch, 2002; Daniault et al., 2016; Pollard et al., 1996). This drives the strong, positive correlations between ADT and the dive metrics, respectively within the WEB (Fig. 4b & 5b and Table 2). Anticyclonic features were also common in other areas of the NAO. For example, around the Azores, more anticyclonic than cyclonic eddies occur (Caldeira and Reis, 2017). Additionally, at the entrance of the Med in the Gulf of Cádiz and over the Seine Abyssal Plain, Mediterranean Outflow Water circulates anticyclonically (De Pascual-Collar et al., 2019). In these regions, ABT spent over 10% of their time at mesopelagic depths (Fig. 4c) and the daily maximum depth of ABT surpassed 400 m (Fig. 5c), resulting in a positive correlation between these dive metrics and ADT (Fig. 4b & 5b and Table 2).

The increased deep diving behavior of ABT in regions with anticyclonic eddies and/or recirculation in the open ocean is consistent with recent studies that show that other top predators utilize anticyclones to access mesopelagic fish communities (e.g., Arostegui et al., 2022; Braun et al., 2019; Gaube et al., 2018, 2017). When the circulation in a region is anticyclonic, waters converge at the surface and are downwelled such that warmer, surface waters reach deeper depths. This is hypothesized to release ectothermic top predators from their thermal constraints and enable them to access what is described by Irigoien et al. (2014) as the largest fish biomass on Earth. However, ABT have the physiological capability to allow for extensive and rapid, deep dives to forage in the mesopelagic deep scattering layer (DSL) (Neill and Stevens, 1974; Stevens et al., 2000). As such, in general, top predators could be using anticyclonic features to feed due to the presence of higher mesopelagic biomass within their boundaries (Della Penna and Gaube, 2020; Wang et al., 2023).

In the NAO, the densest DSLs occur in the NB, which are also amongst the densest, if not the densest, DSLs in the world (Fennell and Rose, 2015). This suggests that ABT are travelling across the NAO in a directed migration to reach an abundant mesopelagic feeding ground and diving deeper to feed on these DSLs. Although no feeding studies have been done in the NB, Devine et al. (2021) found that myctophids and stomiids were the most abundant species in the mesopelagic DSL of anticyclones located in the NB, comprising of over 50% of the total catch. The increased time spent by ABT at mesopelagic depths in the NB suggests that they could either be feeding directly on these mesopelagic fish

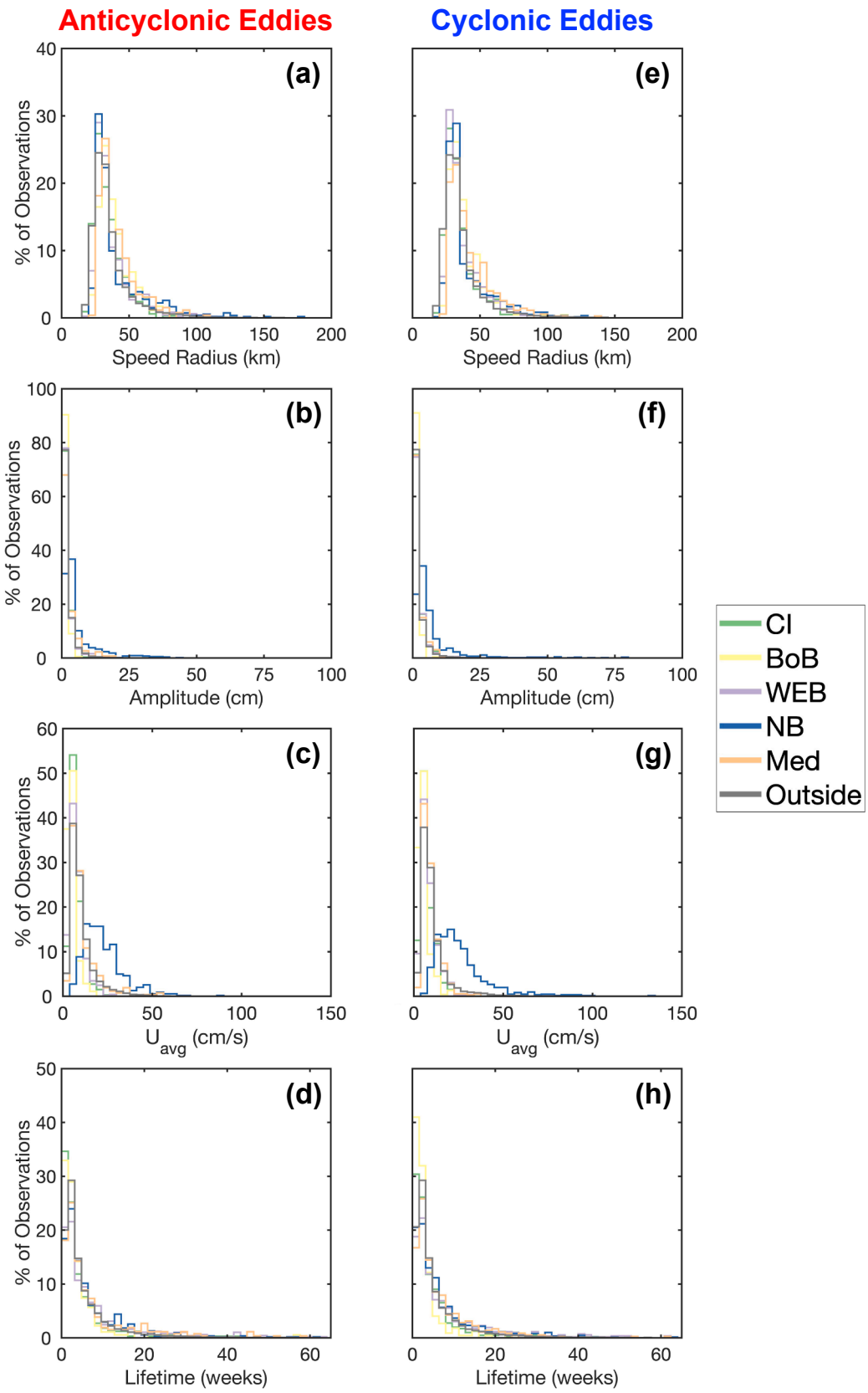

Fig. 9. Histograms of eddy speed radius (km), amplitude (cm), average axial speed (cm/s) and lifetime (weeks) of (a-d) anticyclonic and (e-h) cyclonic eddies within each of the five hotspots (CI: Coastal Ireland, BoB: Bay of Biscay, WEB: West European Basin, NB: Newfoundland Basin, Med: Mediterranean Sea) and outside of these hotspots.

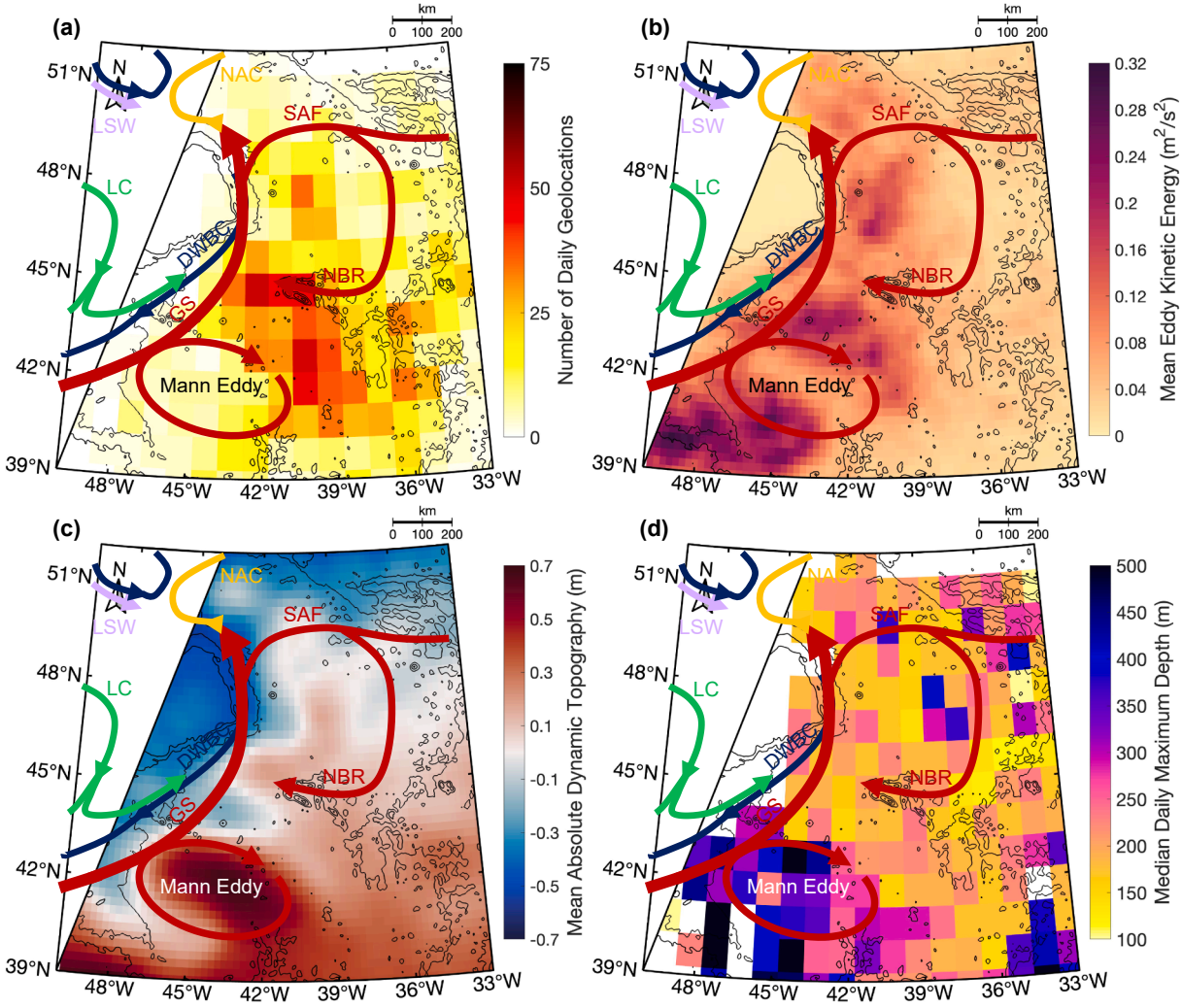

Fig. 10. (a) Number of daily geolocations within 1° × 1° latitude and longitude bins, (b) mean eddy kinetic energy (m^2/s^2), (c) mean absolute dynamic topography (m), and (d) mean daily maximum depth (m) within 1° × 1° latitude and longitude bins in the Newfoundland Basin. Colorbar is cut between 100 m and 500 m. Isobaths are drawn every 1000 m between 2000 and 5000 m. Schematic diagram of the North Atlantic circulation, adapted from Daniault et al. (2016) and Mertens et al. (2014), is overlayed on each panel. Labeled water masses and currents include Deep Western Boundary Current (DWBC, blue line), Gulf Stream (GS, red line), Labrador Current (LC, green line), Labrador Sea Water (LSW, purple line), Mann Eddy, Newfoundland Basin Recirculation (NBR, red line), North Atlantic Current (NAC, orange and red lines), and Subarctic Front (SAF, red line).

Table 4
Overview of eddy statistics in and outside of the five hotspots (CI: Coastal Ireland, BoB: Bay of Biscay, WEB: West European Basin, NB: Newfoundland Basin, Med: Mediterranean Sea). Counts and median (± median absolute deviation) values are reported for anticyclones (ACE) and cyclones (CE). * indicates a significant difference in the median values inside the hotspot from outside of the hotspots at the 5 % level. *p*-values are listed in Tables S9–S16.

	# of realizations		# of unique eddies		L_s (km)		A (cm)		U_{avg} (cm/s)		Lifetime (weeks)	
	ACE	CE	ACE	CE	ACE	CE	ACE	CE	ACE	CE	ACE	CE
CI	4830	6215	329	398	31.6 ± 5.7	31.4 ± 5.4	1.2 ± 0.6	1.3 ± 0.6	6.5 ± 1.9*	6 ± 2.0*	2.4 ± 1.6*	2.7 ± 1.4*
BoB	3394	4086	176	222	36.5 ± 6.2*	34.9 ± 5.5*	0.9 ± 0.3*	0.9 ± 0.3*	4.2 ± 1.1*	4.5 ± 1.2*	2.6 ± 1.1*	2 ± 0.7*
WEB	15,476	15,662	486	521	32.7 ± 5.8	32.4 ± 5.4*	1.3 ± 0.6	1.4 ± 0.7	7 ± 2.3*	7.2 ± 2.5*	4.3 ± 2.9*	4.4 ± 3.0*
NB	16,927	18,554	542	599	33.2 ± 6.0*	33 ± 5.5*	3.4 ± 1.6*	4.1 ± 2.0*	20.3. ± 6.6*	22.5 ± 7.3*	3.8 ± 2.2*	3.9 ± 2.6*
Med	7380	9226	259	352	36.7 ± 6.8*	36.6 ± 7.1*	1.5 ± 0.8*	1.4 ± 0.7	8.2 ± 2.6	8 ± 2.4	3.9 ± 2.4	3.9 ± 2.4
Outside	462,901	464,290	15,096	15,390	32.0 ± 5.8	32 ± 5.7	1.3 ± 0.6	1.3 ± 0.6	8.1 ± 2.8	8.2 ± 2.7	3.3 ± 1.9	3.3 ± 1.9

species or on other animals that may eat these two fish species (Chase, 2002). Along the 20 °W parallel, the WEB corresponds to the highest intensity of the mesopelagic DSL (Peña et al., 2020). While the intensity of the mesopelagic DSL in the WEB is not as high as in the NB (Fennell and Rose, 2015), the WEB could also be an important mesopelagic feeding ground for ABT, hence their increased presence in this region at mesopelagic depths. Though, this may also be due to the absence of a shallow DSL in the WEB (García-Seoane et al., 2023).

4.3. Other foraging grounds off the Coastal Ireland and in the Bay of Biscay

In the CI hotspot, satellite imagery showed positive ADT and high EKE inside the Rockall Trough (Fig. 11c & d). This is the signature of the Rockall Trough Eddy, a semi-permanent, anticyclone formed by the merging of multiple sub-mesoscale coherent vortices whose signature extends below the surface (de Marez et al., 2021; Le Corre et al., 2019;

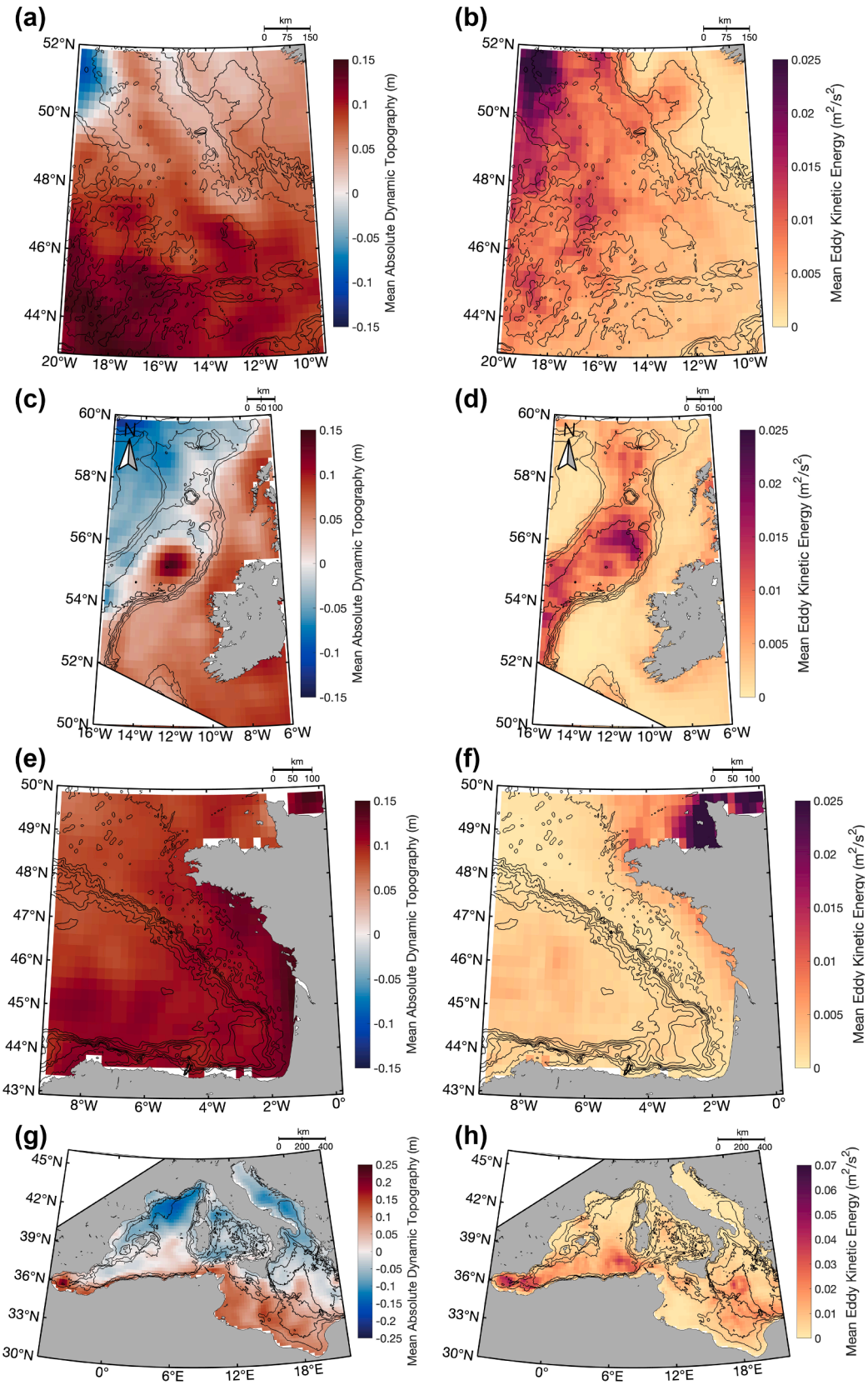

Fig. 11. Mean absolute dynamic topography (m) and mean eddy kinetic energy (m^2/s^2) in the (a & b) West European Basin (WEB), (c & d) Coastal Ireland (CI) hotspot, (e & f) Bay of Biscay (BoB), and (g & h) Mediterranean Sea (Med). Isobaths are drawn in the WEB every 1000 m between 500 and 5500 m, in the CI hotspot every 500 m between 1000 and 3000 m, and in the BoB and Med at 100, 250 and 500 m as well as every 1000 m between 1000 and 4000 m.

Roullet et al., 2014; Solodoch et al., 2021). However, unlike in the open ocean, this anticyclonic feature was not associated with deep diving or extended time at mesopelagic depths as dive metrics were negatively correlated with ADT within this hotspot (Fig. 4b & 5b). ABT spent most of their time at depths between 0 and 5 m as well as 10 and 50 m (Fig. 3a). Less than 1% of their time was spent at mesopelagic depths (Fig. 4a), most of which occurred in the northeast corner of the hotspot (Fig. 4c). Here, the central and southern branches of the warm NAC interact with the cold Iceland–Scotland Overflow Water (Fig. 1). This mixing of warm and cold water masses is similar to what occurs in the areas of the NB and WEB where ABT are diving deeper and spending more time at mesopelagic depths. Overall, the limited time spent in mesopelagic waters is likely because ABT spend most of their time on the continental shelf (Fig. S1), where their maximum depth is constrained to approximately 100 m.

While many large ABT transited through each hotspot, some spent prolonged periods of residency in the BoB similarly to small ABT, who also have local residency patterns within this hotspot (Arregui et al., 2018). In the southeast corner of the BoB, a quasi-stationary ACE centered around 44.5 °N, 4 °W is present in the Spring and Summer. Its lack of climatological signature is due to the seasonal cycle of the slope current in this area, replacing the ACE with a CE in Fall and Winter at the same location (Caballero et al., 2014; Ferrer and Caballero, 2011; Pingree and Le Cann, 1992a, 1992b). Logbook data show that ABT fishing is concentrated within the boundaries of this eddy (Rodríguez-Marín et al., 2003). However, fishing effort peaks in the Summer and thus, catch is primarily comprised of small ABT as large ABT only occupied these waters from Fall to Spring (Fig. 2).

The BoB is an important feeding ground for small ABT (Arregui et al., 2018). Small ABT use water depths between 10 and 50 m in this hotspot more often than in the open ocean. This pattern continues for large ABT (Fig. 3b). As suggested by Arregui et al., (2018) for small ABT, the increased time spent in surface waters by large ABT in the BoB likely reflects the vertical distribution of their prey. High biomass of juvenile European anchovy (*Engraulis encrasicolus*), a major prey item of ABT (Logan et al., 2011), has been recorded in the same area as the seasonal ACE in the BoB, particularly in the top 45 m of the water column during the daytime (Boyra et al., 2013). Increases in anchovy biomass through range expansion due to climate change could result in the expansion of ABT foraging grounds further north beyond the coast of Ireland and BoB in the future (Petitgas et al., 2012).

4.4. Spawning grounds in the Mediterranean Sea

Our tagging efforts off the coast of Ireland were focused on large ABT that were potentially mature and thus expected to migrate to the spawning grounds in the Med. ABT (CFL at entry $\mu \pm \sigma$: 227.3 ± 15.9 cm) in this study visited this hotspot primarily in the Spring and Summer (Fig. 2c & d), with a mid-May mean entry and early-July mean exit (Table S17). As such, fish tagged in this study spent longer in the Med ($\mu \pm \sigma$: 53 ± 30 days; Table S2) than previously reported for the highly migrant subpopulation in the westernmost Med. Both Abascal et al. (2016) and Aranda et al. (2013) reported short residencies in the Med (i.e., between 22 and 39 days). However, only 2 of the 11 ABT tagged by Abascal et al. (2016) traveled east of 2 °E while all 14 ABT that entered the Med in this study crossed this meridian for at least 5 days. Aranda et al. (2013) reported similar exit dates (i.e., between July 3 and 17). However, their tagging occurred within the Med in June (i.e., after the fish had crossed the Strait of Gibraltar), which may have contributed to shorter reported Med residencies. The only fish that traveled to the Med in Aarestrup et al. (2022) entered on May 22 and exited on July 20, which fits within the range of entry and exit dates reported in this study (Table S17).

In the Alboran Sea, just east of the Strait of Gibraltar at the entrance of the Med, ABT dove to depths greater than 250 m (Fig. 5c). Abascal et al. (2016) also observed deep dives over 200 m in this area and suggested that this behavior was in response to quasi-permanent upwelling in the northwestern Alboran Sea. However, we found that the mean ADT clearly showed two nearly permanent anticyclones, known as the Alboran Gyres (Fig. 11g; Pegliasco et al., 2021; Stuhlmacher and Gade, 2020; Wang, 1987) in the same area where the deep diving occurred. Given that the daily maximum depth was positively correlated with ADT in other hotspots, it is possible that ABT could also be utilizing these ACEs to reach mesopelagic prey, which are present in the diet of ABT caught near the Strait of Gibraltar (Aranda et al., 2013).

The presence of ABT was concentrated east of the Alboran Gyres in the Balearic Sea (Fig. 1), where the daily maximum depth of ABT was less than 50 m (Fig. 5c). This aligns with previous findings that suggest the Balearic Sea as one of the principal spawning areas for ABT in the Med and that ABT have a shallower depth distribution on these spawning grounds (Abascal et al., 2016; Aranda et al., 2013; Gordoa et al., 2009; Heinisch et al., 2008). Additionally, in this area of the Med, high abundances of ABT larvae are known to be associated with seasonal anticyclonic structures (Alemany et al., 2010; García et al., 2005; Mariani et al., 2010; Rodriguez et al., 2013; Sabatés et al., 2007). This follows Bakun (2013)'s hypothesis that bluefin tunas may utilize convergent zones to concentrate larvae and increase their retention in optimal habitats. Larvae of ABT and blackfin tuna (*Thunnus atlanticus*) as well as adult ABT exhibiting spawning behavior aggregate on the edges of ACEs near the Loop Current in the Gulf of Mexico, where the western stock of ABT are known to spawn (Cornic and Rooker, 2018; Lindo-Atichati et al., 2012; Muhling et al., 2017; Teo et al., 2007). As such, ABT spawning in the Med may be associated with the edges of ACEs rather than the cores, which could explain why we found no correlation between the daily maximum depth and ADT throughout in this hotspot.

5. Conclusions

In this study, the movement ecology of large ABT in the NAO and Med has emerged more clearly due to the availability of long duration tracks resulting from improved attachment techniques. Here, we showed that ABT tagged off the coast of Ireland concentrate in five oceanographic hotspots: three joined near the East Atlantic coast (CI, BoB, WEB), one mid-ocean region likely used for foraging (NB) and one spawning ground (Med). ABT followed the warm, salty waters of the NAC to travel between regions in the NAO with semi-permanent or permanent anticyclonic features. Depth data indicated that ABT primarily stay in surface waters less than 50 m deep, but often dive into the mesopelagic to forage, especially in regions with anticyclonic features in the open ocean. Some of the tagged ABT migrated to their spawning grounds in the Med in mid-May. They exit this hotspot in early-July, returning to the NAO. Results from this study improve our knowledge of large ABT oceanographic preferences, allowing us to fine-tune predictions of where tuna aggregations might occur.

CRediT authorship contribution statement

Camille M.L.S. Pagniello: Conceptualization, Investigation, Formal analysis, Methodology, Software, Visualization, Writing – original draft, Writing – review & editing. **Niall Ó Maoiléidigh:** Conceptualization, Investigation, Funding acquisition, Methodology, Writing – review & editing. **Hugo Maxwell:** Conceptualization, Investigation, Methodology, Writing – review & editing. **Michael R. Castleton:** Data curation, Formal analysis, Methodology, Software. **Emilius A. Aalto:** Writing – review & editing. **Jonathan J. Dale:** Formal analysis, Methodology, Software, Visualization. **Robert J. Schallert:** Methodology. **Michael J. W. Stokesbury:** Methodology. **Ronán Cosgrove:** Methodology. **Simon Dedman:** Conceptualization, Data curation, Software. **Alan Drumm:** Methodology. **Ross O'Neill:** Methodology, Software. **Barbara A. Block:** Conceptualization, Funding acquisition, Methodology, Supervision, Investigation, Writing – review & editing.

Declaration of Competing Interest

The authors declare that they have no known competing financial interests or personal relationships that could have appeared to influence the work reported in this paper.

Data availability

Data will be made available on request.

Acknowledgements

Funding for electronic tagging of Atlantic bluefin tuna was provided by the Marine Institute, Stanford University, TAG A Giant, ICCAT (Atlantic Wide Research Programme for Bluefin Tuna (GBYP)) and the European Maritime and Fisheries Fund (EMFF - Sustainable Fisheries Scheme A3: Innovation Project Ref: 19.SF.A.03 - Tracking Bluefin Tuna caught in Irish waters - Stock status and origin and factors influencing their presence in Irish waters, distribution, and oceanic migrations). Funding for data processing by the Stanford University team was provided by the NOAA Bluefin Tuna Research program and The Ocean Foundation's TAG A Giant Fund and Pure Edge Foundation Grant to Stanford University. C.M.L.S.P was supported in part by the MAC3 Impact Philanthropies.

All tagging was carried out under an Animal Welfare License (Project AE19121/P003) as required under Directive 2010/63 /EU and Irish Government S.I. No. 543 of 2012).

The authors would like to thank A. Molloy, M. Callaghan and D. Edwards for their fishing expertise and enthusiastic support of the tagging programme. Thank you to F. Alemany for his support of the electronic tagging programme and to T. Reimer for an initial draft of the introduction.

The altimetric Mesoscale Eddy Trajectories Atlas products were produced by SSALTO/DUACS and distributed by AVISO+ (https://www.aviso.altimetry.fr/) with support from CNES, in collaboration with IMEDEA.

Appendix A. Supplementary data

Supplementary data to this article can be found online at https://doi.org/10.1016/j.pocean.2023.103135.

References

Aalto, E.A., Dedman, S., Stokesbury, M.J.W., Schallert, R.J., Castleton, M., Block, B.A., 2023. Evidence of bluefin tuna (*Thunnus thynnus*) spawning in the Slope Sea region of the Northwest Atlantic from electronic tags. ICES Journal of Marine Science 861–877. https://doi.org/10.1093/icesjms/fsad015.

Aarestrup, K., Baktoft, H., Birnie-Gauvin, K., Sundelöf, A., Cardinale, M., Quilez-Badia, G., Onandia, I., Casini, M., Nielsen, E.E., Koed, A., Alemany, F., MacKenzie, B. R., 2022. First tagging data on large Atlantic bluefin tuna returning to Nordic waters suggest repeated behaviour and skipped spawning. Scientific Reports 12, 11772. https://doi.org/10.1038/s41598-022-15819-x.

Abascal, F.J., Medina, A., De La Serna, J.M., Godoy, D., Aranda, G., 2016. Tracking bluefin tuna reproductive migration into the Mediterranean Sea with electronic pop-up satellite archival tags using two tagging procedures. Fisheries Oceanography 25, 54–66. https://doi.org/10.1111/fog.12134.

Alemany, F., Quintanilla, L., Velez-Belchí, P., García, A., Cortés, D., Rodríguez, J.M., Fernández de Puelles, M.L., González-Pola, C., López-Jurado, J.L., 2010. Characterization of the spawning habitat of Atlantic bluefin tuna and related species in the Balearic Sea (western Mediterranean). Progress in Oceanography 86, 21–38. https://doi.org/10.1016/j.pocean.2010.04.014.

Aranda, G., Abascal, F.J., Varela, J.L., Medina, A., 2013. Spawning behaviour and post-spawning migration patterns of Atlantic bluefin tuna (*Thunnus thynnus*) ascertained from satellite archival tags. PLoS One1 8, 1–14. https://doi.org/10.1371/journal.pone.0076445.

Arostegui, M.C., Gaube, P., Woodworth-Jefcoats, P.A., Kobayashi, D.R., Braun, C.D., 2022. Anticyclonic eddies aggregate pelagic predators in a subtropical gyre. Nature 609, 535–540. https://doi.org/10.1038/s41586-022-05162-6.

Arregui, I., Galuardi, B., Goñi, N., Lam, C.H., Fraile, I., Santiago, J., Lutcavage, M., Arrizabalaga, H., 2018. Movements and geographic distribution of juvenile bluefin tuna in the Northeast Atlantic, described through internal and satellite archival tags. ICES Journal of Marine Science 75, 1560–1572. https://doi.org/10.1093/icesjms/fsy056.

Bakun, A., 2013. Ocean eddies, predator pits and bluefin tuna: Implications of an inferred "low risk-limited payoff" reproductive scheme of a (former) archetypical top predator. Fish and Fisheries 14, 424–438. https://doi.org/10.1111/faf.12002.

Bauer, R., 2022. RchivalTag: Analyzing Archival Tagging Data. https://doi.org/https://cran.r-project.org/package=RchivalTag.

Belkin, I.M., Cornillon, P.C., Sherman, K., 2009. Fronts in Large Marine Ecosystems. Progress in Oceanography 81, 223–236. https://doi.org/10.1016/j.pocean.2009.04.015.

Bersch, M., 2002. North Atlantic Oscillation–induced changes of the upper layer circulation in the northern North Atlantic Ocean. Journal of Geophysical Research 107, 1–11. https://doi.org/10.1029/2001jc000901.

Bestley, S., Gunn, J.S., Hindell, M.A., 2009. Plasticity in vertical behaviour of migrating juvenile southern bluefin tuna (*Thunnus maccoyii*) in relation to oceanography of the south Indian Ocean. Fisheries Oceanography 18, 237–254. https://doi.org/10.1111/j.1365-2419.2009.00509.x.

Block, B.A., Jonsen, I.D., Jorgensen, S.J., Winship, A.J., Shaffer, S.A., Bograd, S.J., Hazen, E.L., Foley, D.G., Breed, G.A., Harrison, A.-L., Ganong, J.E., Swithenbank, A., Castleton, M., Dewar, H., Mate, B.R., Shillinger, G.L., Schaefer, K.M., Benson, S.R., Weise, M.J., Henry, R.W., Costa, D.P., 2011. Tracking apex marine predator movements in a dynamic ocean. Nature 475, 86–90. https://doi.org/10.1038/nature10082.

Bower, A.S., Lozier, M.S., Gary, S.F., Böning, C.W., 2009. Interior pathways of the North Atlantic meridional overturning circulation. Nature 459, 243–247. https://doi.org/10.1038/nature07979.

Boyra, G., Martínez, U., Cotano, U., Santos, M., Irigoien, X., Uriarte, A., 2013. Acoustic surveys for juvenile anchovy in the Bay of Biscay: abundance estimate as an indicator of the next year's recruitment and spatial distribution patterns. ICES Journal of Marine Science 70, 1354–1368. https://doi.org/10.1093/icesjms/fst096.

Braun, C.D., Gaube, P., Sinclair-Taylor, T.H., Skomal, G.B., Thorrold, S.R., 2019. Mesoscale eddies release pelagic sharks from thermal constraints to foraging in the ocean twilight zone. Proceedings of the National Academy of Sciences of the United States of America 116, 17187–17192. https://doi.org/10.1073/pnas.1903067116.

Caballero, A., Ferrer, L., Rubio, A., Charria, G., Taylor, B.H., Grima, N., 2014. Monitoring of a quasi-stationary eddy in the Bay of Biscay by means of satellite, in situ and model results. Deep. Res. Part II Top. Stud. Oceanogr. 106, 23–37. https://doi.org/10.1016/j.dsr2.2013.09.029.

Caldeira, R.M.A., Reis, J.C., 2017. The Azores confluence zone. Frontiers in Marine Science 4, 1–14. https://doi.org/10.3389/fmars.2017.00037.

Caniaux, G., Prieur, L., Giordani, H., Hernandez, F., Eymard, L., 2001. Observation of the Circulation in the Newfoundland Basin in Winter 1997. Journal of Physical Oceanography 31, 689–710. https://doi.org/10.1175/1520-0485(2001)031<0689:OOTCIT>2.0.CO;2.

Carracedo, L.I., Mercier, H., McDonagh, E., Rosón, G., Sanders, R., Moore, C.M., Torres-Valdés, S., Brown, P., Lherminier, P., Pérez, F.F., 2021. Counteracting Contributions of the Upper and Lower Meridional Overturning Limbs to the North Atlantic Nutrient Budgets: Enhanced Imbalance in 2010. Global Biogeochemical Cycles 35. https://doi.org/10.1029/2020GB006898.

Cermeño, P., Quílez-Badia, G., Ospina-Alvarez, A., Sainz-Trápaga, S., Boustany, A.M., Seitz, A.C., Tudela, S., Block, B.A., 2015. Electronic tagging of Atlantic bluefin tuna (*Thunnus thynnus*, L.) reveals habitat use and behaviors in the Mediterranean Sea. PLoS One1 10. https://doi.org/10.1371/journal.pone.0116638.

Chase, B.C., 2002. Differences in diet of Atlantic bluefin tuna (*Thunnus thynnus*) at five seasonal feeding grounds on the New England continental shelf. Fishery Bulletin 100, 168–180.

Cornic, M., Rooker, J.R., 2018. Influence of oceanographic conditions on the distribution and abundance of blackfin tuna (*Thunnus atlanticus*) larvae in the Gulf of Mexico. Fisheries Research 201, 1–10. https://doi.org/10.1016/j.fishres.2017.12.015.

Cosgrove, R., Stokesbury, M., Browne, D., Boustany, A., Block, B., O'Farrell, M., 2008. Bluefin Tuna Tagging in Irish Waters, in: Fisheries Resource Series. Bord Iascaigh Mhara (Irish Sea Fisheries Board), Dun Laoghaire, Ireland, p. 16.

Daniault, N., Mercier, H., Lherminier, P., Sarafanov, A., Falina, A., Zunino, P., Pérez, F.F., Ríos, A.F., Ferron, B., Huck, T., Thierry, V., Gladyshev, S., 2016. The northern North Atlantic Ocean mean circulation in the early 21st century. Progress in Oceanography 146, 142–158. https://doi.org/10.1016/j.pocean.2016.06.007.

de Marez, C., Le Corre, M., Gula, J., 2021. The influence of merger and convection on an anticyclonic eddy trapped in a bowl. Ocean Model 167, 101874. https://doi.org/10.1016/j.ocemod.2021.101874.

De Metrio, G., Arnold, G.P., de la Serna, J.M., Megalofonou, P., Buckley, A.A., Pappalepore, M., 2001. Further results of tagging Mediterranean bluefin tuna with pop-up satellite-detected tags. Collect. Vol. Sci. Pap. ICCAT 52, 776–783.

De Metrio, G., Arnold, G.P., Block, B.A., de la Serna, J.M., Deflorio, M., Cataldo, M., Yannopoulos, C., Megalofonou, P., Beemer, S., Farwell, C., Seitz, A., 2002. Behaviour of post-spawning Atlantic bluefin tuna tagged with pop-up satellite tags in the Mediterranean and eastern Atlantic. Collect. Vol. Sci. Pap. ICCAT 54, 415–424.

De Metrio, G., Arnold, G.P., de la Serna, J.M., Block, B.A., Megalofonou, P., Lutcavage, M., Oray, I., Deflorio, M., 2005. Movements of bluefin tuna (*Thunnus Thynnus* L.) tagged in the Mediterranean Sea with pop-up satellite tags 58, 1337–1340.

De Pascual-Collar, Á., Sotillo, M.G., Levier, B., Aznar, R., Lorente, P., Amo-Baladrón, A., Álvarez-Fanjul, E., 2019. Regional circulation patterns of Mediterranean Outflow Water near the Iberian and African continental slopes. Ocean Science 15, 565–582. https://doi.org/10.5194/os-15-565-2019.

Della Penna, A., Gaube, P., 2020. Mesoscale Eddies Structure Mesopelagic Communities. Frontiers in Marine Science 7, 1–9. https://doi.org/10.3389/fmars.2020.00454.

Devine, B., Fennell, S., Themelis, D., Fisher, J.A.D., 2021. Influence of anticyclonic, warm-core eddies on mesopelagic fish assemblages in the Northwest Atlantic Ocean. Deep. Res. Part I Oceanogr. Res. Pap. 173, 103555 https://doi.org/10.1016/j.dsr.2021.103555.

Falkowski, P.G., Ziemann, D., Kolber, Z., Bienfang, P.K., 1991. Role of eddy pumping in enhancing primary production in the ocean. Nature 352, 55–58. https://doi.org/10.1038/352055a0.

Fennell, S., Rose, G., 2015. Oceanographic influences on Deep Scattering Layers across the North Atlantic. Deep. Res. Part I Oceanogr. Res. Pap. 105, 132–141. https://doi.org/10.1016/j.dsr.2015.09.002.

Ferrer, L., Caballero, A., 2011. Eddies in the Bay of Biscay: A numerical approximation. Journal of Marine Systems 87, 133–144. https://doi.org/10.1016/j.jmarsys.2011.03.008.

Ferter, K., Tracey, S., Hinriksson, J., Bjelland, O., Onandia, I., Nøttestad, L., 2019. Tagging of Atlantic bluefin tuna (*Thunnus thynnus*) with pop-up satellite archival tags (PSAT) in western Norway during 2018.

Fromentin, J.-M., Lopuszanski, D., 2014. Migration, residency, and homing of bluefin tuna in the western Mediterranean Sea. ICES Journal of Marine Science 71, 510–518. https://doi.org/10.1093/icesjms/fst157.

Fujioka, K., Fukuda, H., Tei, Y., Okamoto, S., Kiyofuji, H., Furukawa, S., Takagi, J., Estess, E., Farwell, C.J., Fuller, D.W., Suzuki, N., Ohshimo, S., Kitagawa, T., 2018. Spatial and temporal variability in the trans-Pacific migration of Pacific bluefin tuna (*Thunnus orientalis*) revealed by archival tags. Progress in Oceanography 162, 52–65. https://doi.org/10.1016/j.pocean.2018.02.010.

García, A., Alemany, F., Velez-Belchí, P., López Jurado, J.L., Cortés, D., Serna, J.M.D.L., González Pola, C., Rodríguez, J.M., Jansá, J., Ramírez, T., 2005. Characterization of the Bluefin Tuna Spawning Habitat Off the Balearic Archipelago in Relation To Key Hydrographic. Collect. Vol. Sci. Pap. ICCAT 58, 535–549.

García-Ibáñez, M.I., Pardo, P.C., Carracedo, L.I., Mercier, H., Lherminier, P., Ríos, A.F., Pérez, F.F., 2015. Structure, transports and transformations of the water masses in the Atlantic Subpolar Gyre. Progress in Oceanography 135, 18–36. https://doi.org/10.1016/j.pocean.2015.03.009.

García-Seoane, E., Klevjer, T., Mork, K.A., Agersted, M.D., Macaulay, G.J., Melle, W., 2023. Acoustic micronektonic distribution and density is structured by macroscale oceanographic processes across 17–48° N latitudes in the North Atlantic Ocean. Scientific Reports 13, 1–16. https://doi.org/10.1038/s41598-023-30653-5.

Gary, S.F., Susan Lozier, M., Böning, C.W., Biastoch, A., 2011. Deciphering the pathways for the deep limb of the Meridional Overturning Circulation. Deep. Res. Part II Top. Stud. Oceanogr. 58, 1781–1797. https://doi.org/10.1016/j.dsr2.2010.10.059.

Gaube, P., Barceló, C., McGillicuddy, D.J., Domingo, A., Miller, P., Giffoni, B., Marcovaldi, N., Swimmer, Y., 2017. The use of mesoscale eddies by juvenile loggerhead sea turtles (*Caretta caretta*) in the southwestern Atlantic. PLoS One1 12. https://doi.org/10.1371/journal.pone.0172839.

Gaube, P., Braun, C.D., Lawson, G.L., McGillicuddy, D.J., Penna, A.D., Skomal, G.B., Fischer, C., Thorrold, S.R., 2018. Mesoscale eddies influence the movements of mature female white sharks in the Gulf Stream and Sargasso Sea. Scientific Reports 8, 1–8. https://doi.org/10.1038/s41598-018-25565-8.

Gibbs, R., Collette, B., 1967. Comparative anatomy and systematics of the tunas, genus *Thunnus*. Fishery Bulletin 66, 65–130.

Gordoa, A., Olivar, M.P., Arevalo, R., Viñas, J., Molí, B., Illas, X., 2009. Determination of Atlantic bluefin tuna (*Thunnus thynnus*) spawning time within a transport cage in the western Mediterranean. ICES Journal of Marine Science 66, 2205–2210. https://doi.org/10.1093/icesjms/fsp211.

Heinisch, G., Corriero, A., Medina, A., Abascal, F.J., De La Serna, J.M., Vassallo-Agius, R., Ríos, A.B., García, A., De La Gándara, F., Fauvel, C., Bridges, C.R., Mylonas, C.C., Karakulak, S.F., Oray, I., De Metrio, G., Rosenfeld, H., Gordin, H., 2008. Spatial-temporal pattern of bluefin tuna (*Thunnus thynnus* L. 1758) gonad maturation across the Mediterranean Sea. Marine Biology 154, 623–630. https://doi.org/10.1007/s00227-008-0955-6.

Heywood, K.J., McDonagh, E.L., White, M., a,, 1994. Eddy kinetic energy of the North Atlantic subpolar gyre from satellite altimetry. Journal of Geophysical Research 99, 22525–22539. https://doi.org/10.1029/94JC01740.

Hill, R.D., 1994. Theory of geolocation by light levels. In: Le Boeuf, B.J., Laws, R.M. (Eds.), Elephant Seals: Population Ecology, Behavior and Physiology. University of California Press, Berkeley, California, pp. 227–236.

Horton, T.W., Block, B.A., Drumm, A., Hawkes, L.A., O'Cuaig, M., Maoiléidigh, Ó., N., O'Neill, R., Schallert, R.J., Stokesbury, M.J.W., Witt, M.J.,, 2020. Tracking Atlantic bluefin tuna from foraging grounds off the west coast of Ireland. ICES Journal of Marine Science 77, 2066–2077. https://doi.org/10.1093/icesjms/fsaa090.

Irigoien, X., Klevjer, T.A., Røstad, A., Martinez, U., Boyra, G., Acuña, J.L., Bode, A., Echevarria, F., Gonzalez-Gordillo, J.I., Hernandez-Leon, S., Agusti, S., Aksnes, D.L., Duarte, C.M., Kaartvedt, S., 2014. Large mesopelagic fishes biomass and trophic efficiency in the open ocean. Nature Communications 5, 3271. https://doi.org/10.1038/ncomms4271.

Jonsen, I.D., Flemming, J.M., Myers, R.A., 2005. Robust state-space modeling of animal movement data. Ecology 86, 2874–2880. https://doi.org/10.1890/04-1852.

Keates, T.R., Hazen, E.L., Holser, R.R., Fiechter, J., Bograd, S.J., Robinson, P.W., Gallo-Reynoso, J.P., Costa, D.P., 2022. Foraging behavior of a mesopelagic predator, the northern elephant seal, in northeastern Pacific eddies. Deep. Res. Part I Oceanogr. Res. Pap. 189, 103866 https://doi.org/10.1016/j.dsr.2022.103866.

Kitagawa, T., Kimura, S., Nakata, H., Yamada, H., Nitta, A., Sasai, Y., Sasaki, H., 2009. Immature Pacific bluefin tuna, *Thunnus orientalis*, utilizes cold waters in the Subarctic Frontal Zone for trans-Pacific migration. Environmental Biology of Fishes 84, 193–196. https://doi.org/10.1007/s10641-008-9409-8.

Klein, B., Siedler, G., 1989. On the origin of the Azores Current. Journal of Geophysical Research 94, 6159–6168. https://doi.org/10.1029/JC094iC05p06159.

Krauss, W., 1986. The North Atlantic Current. Journal of Geophysical Research 91, 5061. https://doi.org/10.1029/JC091iC04p05061.

Lawson, G., Castleton, M., Block, B., 2010. Movements and diving behavior of Atlantic bluefin tuna *Thunnus thynnus* in relation to water column structure in the northwestern Atlantic. Marine Ecology Progress Series 400, 245–265. https://doi.org/10.3354/meps08394.

Le Corre, M., Gula, J., Smilenova, A., Houpert, L., 2019. On the dynamics of a deep quasi-permanent anticylonic eddy in the Rockall Trough, in: 24ème Congrès Français de Mécanique. Association Français de Mécanique, Brest, France, p. 12.

Lindo-Atichati, D., Bringas, F., Goni, G., Muhling, B., Muller-Karger, F.E., Habtes, S., 2012. Varying mesoscale structures influence larval fish distribution in the northern Gulf of Mexico. Marine Ecology Progress Series 463, 245–257. https://doi.org/10.3354/meps09860.

Logan, J.M., Rodríguez-Marín, E., Goñi, N., Barreiro, S., Arrizabalaga, H., Golet, W., Lutcavage, M., 2011. Diet of young Atlantic bluefin tuna (*Thunnus thynnus*) in eastern and western Atlantic foraging grounds. Marine Biology 158, 73–85. https://doi.org/10.1007/s00227-010-1543-0.

Luo, J., Ault, J.S., Shay, L.K., Hoolihan, J.P., Prince, E.D., Brown, C.A., Rooker, J.R., 2015. Ocean heat content reveals secrets of Fish Migrations. PLoS One1 10, 1–19. https://doi.org/10.1371/journal.pone.0141101.

MacKenzie, B.R., Aarestrup, K., Birnie-Gauvin, K., Cardinale, M., Casini, M., Harkes, I., Onandia, I., Quilez-Badia, G., Sundelöf, A., 2020. Electronic tagging of adult bluefin tunas by sport fishery in the Skagerrak, 2017. Collect. Vol. Sci. Pap. ICCAT 76, 650–664.

Mann, C.R., 1967. The termination of the Gulf Stream and the beginning of the North Atlantic Current. Deep. Res. Oceanogr. Abstr. 14, 337–359. https://doi.org/10.1016/0011-7471(67)90077-0.

Ó Maoiléidigh, N., Connolly, P., Drumm, A., O'Neill, R., Maxwell, H., Ó'Cuaig, M., Cooney, J., Bunn, R., Stokesbury, M., Schallert, R., Block, B., Horton, T., 2016. Atlantic Bluefin Tuna Tagging Programme in Ireland 2016.

Mariani, P., MacKenzie, B.R., Iudicone, D., Bozec, A., 2010. Modelling retention and dispersion mechanisms of bluefin tuna eggs and larvae in the northwest Mediterranean Sea. Progress in Oceanography 86, 45–58. https://doi.org/10.1016/j.pocean.2010.04.027.

Mason, E., Pascual, A., McWilliams, J.C., 2014. A new sea surface height-based code for oceanic mesoscale eddy tracking. J. Atmos. Ocean. Technol. 31, 1181–1188. https://doi.org/10.1175/JTECH-D-14-00019.1.

Mauzole, Y.L., 2022. Objective delineation of persistent SST fronts based on global satellite observations. Remote Sensing of Environment 269, 112798. https://doi.org/10.1016/j.rse.2021.112798.

McKinney, R., Gibbon, J., Wozniak, E., Galland, G., 2020. Netting Billions 2020: A Global Tuna Valuation.

Mertens, C., Rhein, M., Walter, M., Böning, C.W., Behrens, E., Kieke, D., Steinfeldt, R., Stöber, U., 2014. Circulation and transports in the Newfoundland Basin, western subpolar North Atlantic. J. Geophys. Res. Ocean. 119, 7772–7793. https://doi.org/10.1002/2014JC010019.

Muhling, B.A., Lamkin, J.T., Alemany, F., García, A., Farley, J., Ingram, G.W., Berastegui, D.A., Reglero, P., Carrion, R.L., 2017. Reproduction and larval biology in tunas, and the importance of restricted area spawning grounds. Reviews in Fish Biology and Fisheries 27, 697–732. https://doi.org/10.1007/s11160-017-9471-4.

Neill, W.H., Stevens, E.D., 1974. Thermal Inertia versus Thermoregulation in "Warm" Turtles and Tunas. Science (80-.). 184, 1008–1010. https://doi.org/10.1126/science.184.4140.1008.

Pegliasco, C., Chaigneau, A., Morrow, R., Dumas, F., 2021. Detection and tracking of mesoscale eddies in the Mediterranean Sea: A comparison between the Sea Level Anomaly and the Absolute Dynamic Topography fields. Adv. Sp. Res. 68, 401–419. https://doi.org/10.1016/j.asr.2020.03.039.

Pegliasco, C., Delepoulle, A., Mason, E., Morrow, R., Faugère, Y., Dibarboure, G., 2022. META3.1exp: a new global mesoscale eddy trajectory atlas derived from altimetry. Earth System Science Data 14, 1087–1107. https://doi.org/10.5194/essd-14-1087-2022.

Peña, M., Cabrera-Gámez, J., Domínguez-Brito, A.C., 2020. Multi-frequency and light-avoiding characteristics of deep acoustic layers in the North Atlantic. Marine Environmental Research 154, 104842. https://doi.org/10.1016/j.marenvres.2019.104842.

Petitgas, P., Alheit, J., Peck, M.A., Raab, K., Irigoien, X., Huret, M., Van Der Kooij, J., Pohlmann, T., Wagner, C., Zarraonaindia, I., Dickey-Collas, M., 2012. Anchovy population expansion in the North Sea. Marine Ecology Progress Series 444, 1–13. https://doi.org/10.3354/meps09451.

Pingree, R.D., Le Cann, B., 1992a. Three anticyclonic slope water oceanic eDDIES (SWODDIES) in the Southern Bay of Biscay in 1990. Deep Sea Res. Part A. Oceanogr. Res. Pap. 39, 1147–1175. https://doi.org/10.1016/0198-0149(92)90062-X.

Pingree, R.D., Le Cann, B., 1992b. Anticyclonic eddy X91 in the southern Bay of Biscay, May 1991 to February 1992. Journal of Geophysical Research 97, 14353–14367. https://doi.org/10.1029/92JC01181.

Pollard, R.T., Griffiths, M.J., Cunningham, S.A., Read, J.F., Pérez, F.F., Ríos, A.F., 1996. Vivaldi 1991 - A study of the formation, circulation and ventilation of Eastern North Atlantic Central Water. Progress in Oceanography 37, 167–172. https://doi.org/10.1016/S0079-6611(96)00008-0.

Porch, C.E., Bonhommeau, S., Diaz, G.A., Arrizabalaga, H., Melvin, G., 2019. The Journey from Overfishing to Sustainability for Atlantic bluefin tuna, *Thunnus thynnus*, in: Block, B.A. (Ed.), The Future of Bluefin Tunas: Ecology, Fisheries Management, and Conservation. Johns Hopkins University Press, pp. 15–57. https://doi.org/10.1353/book.67470.

Quílez-Badia, G., Ospina-Alvarez, A., Trápaga, S.S., Di Natale, A., Abrid, N., Cermeño, P., Tudela, S., 2015. The WWF/GBYP multi-annual bluefin tuna electronic tagging

program (2008–2013): repercussions for management. Collect. Vol. Sci. Pap. ICCAT 71, 1789–1802.
Racapé, V., Thierry, V., Mercier, H., Cabanes, C., 2019. ISOW Spreading and Mixing as Revealed by Deep-Argo Floats Launched in the Charlie-Gibbs Fracture Zone. J. Geophys. Res. Ocean. 124, 6787–6808. https://doi.org/10.1029/2019JC015040.
Read, J.F., Pollard, R.T., Miller, P.I., Dale, A.C., 2010. Circulation and variability of the North Atlantic Current in the vicinity of the Mid-Atlantic Ridge. Deep. Res. Part I Oceanogr. Res. Pap. 57, 307–318. https://doi.org/10.1016/j.dsr.2009.11.010.
Rhein, M., Steinfeldt, R., Kieke, D., Stendardo, I., Yashayaev, I., 2017. Ventilation variability of Labrador Sea Water and its impact on oxygen and anthropogenic carbon: a review. Philos. Trans. R. Soc. A Math. Phys. Eng. Sci. 375, 1–17. https://doi.org/10.1098/rsta.2016.0321.
Richardson, P.L., 1993. A census of eddies observed in North Atlantic SOFAR float data. Progress in Oceanography 31, 1–50. https://doi.org/10.1016/0079-6611(93)90022-6.
Richardson, D.E., Marancik, K.E., Guyon, J.R., Lutcavage, M.E., Galuardi, B., Lam, C.H., Walsh, H.J., Wildes, S., Yates, D.A., Hare, J.A., 2016. Discovery of a spawning ground reveals diverse migration strategies in Atlantic bluefin tuna (*Thunnus thynnus*). Proceedings of the National Academy of Sciences of the United States of America 113, 3299–3304. https://doi.org/10.1073/pnas.1525636113.
Rodriguez, J.M., Alvarez, I., Lopez-Jurado, J.L., Garcia, A., Balbin, R., Alvarez-Berastegui, D., Torres, A.P., Alemany, F., 2013. Environmental forcing and the larval fish community associated to the Atlantic bluefin tuna spawning habitat of the Balearic region (Western Mediterranean), in early summer 2005. Deep. Res. Part I Oceanogr. Res. Pap. 77, 11–22. https://doi.org/10.1016/j.dsr.2013.03.002.
Rodríguez-Marín, E., Arrizabalaga, H., Ortiz, M., Rodríguez-Cabello, C., Moreno, G., Kell, L.T., 2003. Standardization of bluefin tuna, *Thunnus thynnus*, catch per unit effort in the baitboat fishery of the Bay of Biscay (Eastern Atlantic). ICES Journal of Marine Science 60, 1216–1231. https://doi.org/10.1016/S1054-3139(03)00139-5.
Roessler, A., Rhein, M., Kieke, D., Mertens, C., 2015. Long-term observations of North Atlantic Current transport at the gateway between western and eastern Atlantic. J. Geophys. Res. Ocean. 120, 4003–4027. https://doi.org/10.1002/2014JC010662.
Rossby, T., 1996. The North Atlantic Current and surrounding waters: At the crossroads. Reviews of Geophysics 34, 463–481. https://doi.org/10.1029/96RG02214.
Roullet, G., Capet, X., Maze, G., 2014. Global interior eddy available potential energy diagnosed from Argo floats. Geophysical Research Letters 41, 1651–1656. https://doi.org/10.1002/2013GL059004.
Sabatés, A., Olivar, M.P., Salat, J., Palomera, I., Alemany, F., 2007. Physical and biological processes controlling the distribution of fish larvae in the NW Mediterranean. Progress in Oceanography 74, 355–376. https://doi.org/10.1016/j.pocean.2007.04.017.
Solodoch, A., McWilliams, J.C., Stewart, A.L., Gula, J., Renault, L., 2020. Why does the deep western boundary current "'leak"' around flemish cap? Journal of Physical Oceanography 50, 1989–2016. https://doi.org/10.1175/JPO-D-19-0247.1.
Solodoch, A., Stewart, A.L., McWilliams, J.C., 2021. Formation of anticyclones above topographic depressions. Journal of Physical Oceanography 51, 207–228. https://doi.org/10.1175/JPO-D-20-0150.1.
Stendardo, I., Gruber, N., 2012. Oxygen trends over five decades in the North Atlantic. J. Geophys. Res. Ocean. 117, 1–18. https://doi.org/10.1029/2012JC007909.
Stendardo, I., Rhein, M., Hollmann, R., 2016. A high resolution salinity time series 1993–2012 in the North Atlantic from Argo and Altimeter data. J. Geophys. Res. Ocean. 121, 2523–2551. https://doi.org/10.1002/2015JC011439.
Stendardo, I., Rhein, M., Steinfeldt, R., 2020. The North Atlantic Current and its Volume and Freshwater Transports in the Subpolar North Atlantic, Time Period 1993–2016. J. Geophys. Res. Ocean. 125 https://doi.org/10.1029/2020JC016065.
Stevens, E.D., Kanwisher, J.W., Carey, F.G., 2000. Muscle temperature in free-swimming giant Atlantic bluefin tuna (*Thunnus thynnus* L.). Journal of Thermal Biology 25, 419–423. https://doi.org/10.1016/S0306-4565(00)00004-8.
Stokesbury, M.J.W., Cosgrove, R., Boustany, A., Browne, D., Teo, S.L.H., O'Dor, R.K., Block, B.A., 2007. Results of satellite tagging of Atlantic bluefin tuna, *Thunnus thynnus*, off the coast of Ireland. Hydrobiologia 582, 91–97. https://doi.org/10.1007/s10750-006-0552-y.
Stuhlmacher, A., Gade, M., 2020. Statistical analyses of eddies in the Western Mediterranean Sea based on Synthetic Aperture Radar imagery. Remote Sensing of Environment 250, 112023. https://doi.org/10.1016/j.rse.2020.112023.
Teo, S.L.H., Boustany, A., Blackwell, S., Walli, A., Weng, K.C., Block, B.A., 2004. Validation of geolocation estimates based on light level and sea surface temperature from electronic tags. Marine Ecology Progress Series 283, 81–98. https://doi.org/10.3354/meps283081.
Teo, S.L.H., Boustany, A.M., Block, B.A., 2007. Oceanographic preferences of Atlantic bluefin tuna, *Thunnus thynnus*, on their Gulf of Mexico breeding grounds. Marine Biology 152, 1105–1119. https://doi.org/10.1007/s00227-007-0758-1.
Tudela, S., Trápaga, S.S., Cermeño, P., Hidas, E., Graupera, E., Quilez-Badia, G., 2011. Bluefin tuna migratory behavior in the western and central Mediterranean Sea revealed by electronic tags. Collect. Vol. Sci. Pap. ICCAT 66, 1157–1169.
Walli, A., Teo, S.L.H., Boustany, A., Farwell, C.J., Williams, T., Dewar, H., Prince, E., Block, B.A., 2009. Seasonal movements, aggregations and diving behavior of Atlantic bluefin tuna (*Thunnus thynnus*) revealed with archival tags. PLoS One1 4. https://doi.org/10.1371/journal.pone.0006151.
Wang, D.-P., 1987. The strait surface outflow. J. Geophys. Res. Ocean. 92, 807–825. https://doi.org/10.1029/JC092iC10p10807.
Wang, Y., Zhang, J., Yu, J., Wu, Q., Sun, D., 2023. Anticyclonic mesoscale eddy induced mesopelagic biomass hotspot in the oligotrophic ocean. Journal of Marine Systems 237, 103831. https://doi.org/10.1016/j.jmarsys.2022.103831.
Wilson, S., Block, B., 2009. Habitat use in Atlantic bluefin tuna *Thunnus thynnus* inferred from diving behavior. Endangered Species Research 10, 355–367. https://doi.org/10.3354/esr00240.
Wilson, S.G., Lutcavage, M.E., Brill, R.W., Genovese, M.P., Cooper, A.B., Everly, A.W., 2005. Movements of bluefin tuna (*Thunnus thynnus*) in the northwestern Atlantic Ocean recorded by pop-up satellite archival tags. Marine Biology 146, 409–423. https://doi.org/10.1007/s00227-004-1445-0.
Wilson, S.G., Jonsen, I.D., Schallert, R.J., Ganong, J.E., Castleton, M.R., Spares, A.D., Boustany, A.M., Stokesbury, M.J.W., Block, B.A., 2015. Tracking the fidelity of Atlantic bluefin tuna released in Canadian waters to the Gulf of Mexico spawning grounds. Canadian Journal of Fisheries and Aquatic Sciences 72, 1700–1717. https://doi.org/10.1139/cjfas-2015-0110.